arXiv:astro-ph/0610014v1 30 Sep 2006

The Lack of Gamma-Ray Bursts from Population III Binaries

Krzysztof Belczynski[1,2], Tomasz Bulik[3,4] Alexander Heger[5,6] and Chris Fryer[7,8]

[1] *New Mexico State University, Dept. of Astronomy, 1320 Frenger Mall, Las Cruces, NM 88003*

[2] *Tombaugh Fellow*

[3] *Astronomical Observatory, Warsaw University, Al. Ujazdowskie 4, 00-478, Warsaw, Poland*

[4] *Nicolaus Copernicus Astronomical Center, Bartycka 18, 00-716 Warszawa, Poland*

[5] *Theoretical Astrophysics, Los Alamos National Laboratory, Los Alamos, NM 87545*

[6] *Department of Astronomy and Astrophysics, University of California, Santa Cruz, CA 95064*

[7] *Computer and Computational Science, Los Alamos National Laboratory, Los Alamos, NM 87545*

[8] *Physics Department, University of Arizona, Tucson, AZ, 85721*

kbelczyn@nmsu.edu,tb@astrouw.edu.pl,aheger@lanl.gov,fryer@lanl.gov

ABSTRACT

We study the evolution of first star (Population III) binaries. Under specific conditions, these stars may produce high redshift gamma-ray bursts (GRBs). We demonstrate that the occurrence rate of GRBs does not depend sensitively on evolutionary parameters in the population synthesis models. We show that the first binaries may form a very small group ($\lesssim 1\%$) of fast rotating stars through binary tidal interactions that make GRBs. This finding is contrary to the Bromm & Loeb assumption that *all* stars in close Population III binaries will be spun up by tides and produce a GRB. We find that there is simply not enough fast rotating stars in Population III binaries to expect detection with *SWIFT*. Predicted detection rates, even with very optimistic assumptions on binary fraction, evolutionary parameters and GRB detection, are very small: $\sim 0.1 - 0.01\mathrm{yr}^{-1}$.

Subject headings: binaries: general — gamma rays: bursts — stars: formation

1. Introduction

Population III stars are formed out of a pristine, metal free gas made in the big bang. These are the first stars in the universe and most of these stars have likely formed at a

redshift of $z \gtrsim 10$. To collapse and form stars in this metal-free environment, with its cooling dominated by H_2, clouds must be larger than in metal-rich environs. Current simulations indicate that an initial mass function of Population III stars is expected to be top heavy with a large fraction of the mass above $100\,M_\odot$ (Larson 1998; Nakamura & Umemura 2001; Abel, Bryan, & Norman 2002; Bromm, Coppi, & Larson 2002; Chabrier 2003), though somewhat less massive, but still massive, stars could form in relic HII regions (O'Shea et al. 2005). Metal free stars also have much weaker (if winds) and hence, much less mass loss than current stellar populations (Kudritzki 2002) and do not show strong pulsational instabilities that could lead to strong mass loss for initial masses up to 500-1000 $M_\odot$ (Baraffe, Heger & Woosley 2001). That is, not only are these stars born massive, but they also keep most of their mass till their late evolution stages, and a large fraction of them form black holes. There are also calculations that indicate that these stars could have mass loss originating from high rotation (e.g., Marigo 2001).

The evolution of metal free stars has been investigated by several authors (e.g., Woosley, Heger, & Weaver 2002; Chieffi & Limongi 2002; Umeda & Nomoto 2002). For Population III stars, the pair instability is important, and it leads to a complete disruption of stars with initial masses between 140 and 260 $M_\odot$ (Bond et al. 1984; Heger & Woosley 2002). Below this mass range, pair instabilities lead to pulsations and some mass loss, while above $260\,M_\odot$, the stars collapse directly to form black holes (Fryer, Woosley & Heger 2001). Population III stars are a primary source of ionizing photons in the early universe and, if they explode, can very quickly enrichment the interstellar medium with metals. The traces of this ionization have been measured by the Wilkinson Microwave Anisotropy Probe (Kogut 2003; Cen 2003; Wyithe & Loeb 2003a, 2003b).

As every known stellar population contains a significant fraction of binary and multiple stars, it is interesting to ask if it was the case for the Population III stars as well. The results of numerical simulation show that metal free clouds with significant angular momentum form binaries (Saigo, Matsumoto & Umemura 2004). Thus it is likely that Population III stars formed in binaries, however, this issue is still a subject of discussion (see Ripamonti & Abel 2004). The evolution of Population III binaries has been first addressed by Belczynski, Bulik & Rudak (2004), who considered the possibility of forming double black hole binaries as a result of Population III binary evolution. The coalescences of such binaries may be detectable by gravitational wave detectors such as LIGO and VIRGO (Kulczycki et al. 2006). Formation of double black hole binaries from single Population III stars through dynamical interactions and corresponding LIGO signal was also considered (Wyithe & Loeb 2004).

Gamma-ray bursts may be a different observational manifestation of Population III

stars. The observed population of long soft GRBs extends to the redshifts above 6. GRBs from higher redshifts are expected to be detectable by current instruments, and so are their afterglows (Lamb & Reichart 2000). The collapsar model (Woosley 1993; MacFadyen & Woosley 1999) seems to match many of the observed qualities of long duration GRBs: burst location in star-forming galaxies and/or star-forming regions in galaxies (Fruchter et al. 1999; Vreeswijk et al. 2001) and the concurrent production of supernovae in the GRB explosion (e.g., Galama et al. 1998). Moreover, GRBs host galaxies tend to be metal poor (Stanek et al. 2006). The main requirements in the collapsar scenario are that *(i)* the star loses its extended envelope, so the relativistic jet can punch through the compact core of a collapsing star on a timescale comparable to a typical timescale of long-soft GRB (Fryer, Woosley & Hartmann 1999), *(ii)* the star retains, or attains, a significant amount of angular momentum, so that a self-supporting torus may form around a black hole during core collapse. Given the high masses of Population III stars at collapse, one might expect Population III stars to produce a lot of GRBs. However, if Population III stars lose no or only very little mass in stellar winds[1], they retain their hydrogen envelopes and hence do not satisfy requirement *(iii)*; (see also Heger et al. 2003). Binary evolution can both help remove the hydrogen envelope (through stripping in Roche lobe overflow) and spin-up binary components.

The binary scenario for Population III GRBs has been considered by Lloyd-Ronning et al. (2002) who studied the dependence of GRB formation on metallicity and later by Bromm & Loeb (2006) who calculated the SWIFT detection rate using a simplified analytical approach to binary evolution. Although Lloyd-Ronning et al. (2002) found only mild or no increase in the ratio of GRBs to SNe for Population III stars, Bromm & Loeb (2006) argued that Population III stars may significantly enhance (in addition to Population I/II progenitors) the rate of GRBs observed at high redshifts. However, simplifications in both Lloyd-Ronning et al. (2002) and Bromm & Loeb (2006) evolutionary models (e.g., they did not calculate the angular momentum of the collapsing star) limited the extent at which these calculations could really estimate the GRB rate.

In this paper we investigate evolutionary scenarios leading to Population III collapsars in binary systems focusing on progenitors spin evolution. We use detailed stellar models for the evolution of Population III stars and follow some basic binary processes important for the angular momentum evolution of potential GRB progenitors. The paper is organized as follows: in § 2 we present the evolutionary model of Population III stars (singles and binaries), in § 3 we describe the results and Population III GRB rates, and § 4 contains our

[1]Although this would seem to rule out single-star progenitors, stellar evolution theorists have found that rotation-induced mixing can increase the helium layer for fast-spinning single stars, allowing single Population III stars to produce GRBs (Woosley & Heger 2006; Yoon & Langer 2005).

conclusions and a summary.

2. Model Description

To follow the evolution of Population III single stars we use models from Heger & Woosley (2006) for 10-100 solar masses, Scannapieco et al. (2005) for more massive stars, and additionally models for lower mass stars (which extend to late evolutionary stages, i.e., AGB) and some high mass stars ($100 - 500$ $M_\odot$) specifically calculated for this study. The revised model of Belczynski et al. (2004) is used to evolve Population III binaries. Final black hole masses and formation of collapsar GRBs are obtained from Fryer (2006) semi-analytic estimates based on numerical simulations.

2.1. Single Star Evolution

The single star evolution was followed using the KEPLER code (Weaver, Zimmerman, & Woosley 1978), an implicit 1D hydro code. A set of published models was used (Heger & Woosley 2007) and additionally some lower mass (< 10 $M_\odot$) and higher mass (> 100 $M_\odot$) models were calculated. We use an initial primordial composition and assume no mass loss. The models used here do not include effects of rotation on the evolution of a star; the initial angular momentum of Population III binaries is not known. The assumptions for semi-convection are such that the AGB-core collapse transition (off-center neon ignition) occurs at $\gtrsim 10$ $M_\odot$, and the first noticeable pulsational pair instability sets in just below 100 $M_\odot$. One of the big uncertainties of these models is the question of mixing of carbon, made in the convective core during core helium burning, with the hydrogen envelope (see, e.g., Heger, Woosley, Waters 2000; Marigo et al. 2001). The massive star models used here show only moderate mixing and remain relatively compact. However, study of Scannapieco et al. (2005), who varied assumptions on semi-convection and overshoot mixing, showed that a large range of radii at the end of core helium burning is possible for massive stars ($\sim 150 - 250$ $M_\odot$). This constitutes a major uncertainty for Population III stellar models.

The initial stellar radii are taken from the models above and from Schaerer (2002). By the end of the main sequence evolution, stellar radii increase by a factor $\sim 2 - 3$ and, on the giant branch, their radii can increase several orders of magnitude. The expansion of a star is very important since it is this expansion that determines the onset of Roche lobe overflow (RLOF). We use models of Marigo et al. (2001) and Baraffe et al. (2001) to obtain star effective temperature and luminosity at the end of its evolution (maximum radial

expansion), and calculate corresponding radius for a given initial star mass. Initial, zero-age main sequence (ZAMS), radii and maximum radii for stars of different initial mass are shown in Figure 1.

Moment of inertia of a star is calculated from

$$I = k\ M\ R^2 \tag{1}$$

where (dimensionless) coefficients k change with the evolution of star's internal structure and are different for the envelope and the core. For MS stars we use single coefficient $k_{\rm ms} = 0.075$ (polytropic model for massive stars; Lai, Rasio & Shapiro 1993) since there is no well defined core/envelope structure yet. For giants we adopt $k_{\rm env} = 0.1$ (detailed giant models of Hurley, Pols & Tout 2000) and $k_{\rm cor} = k_{\rm He}$, and values for $k_{\rm He}$ are obtained from the detailed models of Population III stars (given below). For exposed helium cores we use $k_{\rm He}$ for the entire star.

Helium core mass is estimated from

$$M_{\rm He} = \begin{cases} 0.4 M_{\rm zams} - 3\ {\rm M}_\odot & M_{\rm zams} < 104\ {\rm M}_\odot \\ 0.542 M_{\rm zams} - 17.8\ {\rm M}_\odot & M_{\rm zams} \geq 104\ {\rm M}_\odot \end{cases} \tag{2}$$

where $M_{\rm zams}$ is an initial (ZAMS) mass of a star in ${\rm M}_\odot$.

Helium core radius is taken from:

$$R_{\rm He} = \begin{cases} -548000\ M_{\rm zams}^2 + 4.92 \times 10^8 M_{\rm zams} + 1.11 \times 10^8\,{\rm cm} & M_{\rm zams} < 450\ {\rm M}_\odot \\ 1.27 \times 10^8 M_{\rm zams} + 0.53 \times 10^{11}\,{\rm cm} & M_{\rm zams} \geq 450\ {\rm M}_\odot. \end{cases} \tag{3}$$

Coefficients $k_{\rm He}$ are taken from Heger & Woosley (2006), and can be approximated by

$$k_{\rm He} = \begin{cases} 3.19 \times 10^{-7} M_{\rm zams}^2 - 0.000341 M_{\rm zams} + 0.3 & M_{\rm zams} < 500\ {\rm M}_\odot \\ 0.209 & M_{\rm zams} \geq 500\ {\rm M}_\odot. \end{cases} \tag{4}$$

Moment of inertia [$g\ cm^2$] of the very inner ($M_{7\rm in} = 7\ {\rm M}_\odot$) part of a star core at the H depletion in the core (end of MS and He core formation) is estimated from

$$\log(I_{7\rm in,He}) = \begin{cases} 53.82 + 0.192\ M_{\rm zams} & M_{\rm zams} < 6.9\ {\rm M}_\odot \\ 55.37 - 0.05\ M_{\rm zams} + 0.0016\ M_{\rm zams}^2 - 0.0000155\ M_{\rm zams}^3 & 6.9 \geq M_{\rm zams} < 45\ {\rm M}_\odot \\ 54.89 + 0.00148\ M_{\rm zams} - 0.0000017\ M_{\rm zams}^2 & 45 \geq M_{\rm zams} < 500\ {\rm M}_\odot \\ 55.2 & M_{\rm zams} \geq 500\ {\rm M}_\odot, \end{cases} \tag{5}$$

while the final value (at Fe core formation and just prior the collapse) is estimated from

$$\log(I_{7\mathrm{in,Fe}}) = \begin{cases} 57.25 & M_{\mathrm{zams}} < 10\ \mathrm{M}_\odot \\ 68.73 - 1.79\ M_{\mathrm{zams}} + 0.0597\ M_{\mathrm{zams}}^2 & 10 \geq M_{\mathrm{zams}} < 15\ \mathrm{M}_\odot \\ 59.79 - 0.36\ M_{\mathrm{zams}} + 0.00416\ M_{\mathrm{zams}}^2 & 15 \geq M_{\mathrm{zams}} < 43\ \mathrm{M}_\odot \\ 52.0 & M_{\mathrm{zams}} \geq 43\ \mathrm{M}_\odot. \end{cases} \quad (6)$$

The above formulas describe the results of numerical simulations with an accuracy better than a few percent.

2.2. Remnant Masses/Supernova Explosions

Whether or not a given collapsing star produces a supernova explosion is still a matter of intense study, but it has been known for quite some time that if one can neglect mass loss, low mass stars are easier to explode than high mass stars. Using his 2-dimensional core-collapse simulations, Fryer (1999) argued that low mass stars would form neutron stars in a supernova explosion, but as the mass increased, the explosion would become weaker and the fallback of ejecta would collapse the compact remnant to a black hole. Even more massive stars would not produce a supernova explosion at all. Assuming supernovae are driven by energy stored in the convective region between the surface of the proto-neutron star and the accretion shock, Fryer (2006a) developed a semi-analytic means to estimate the explosion energy and final remnant mass of the collapsing star as a function of the stellar structure. Figure 2 shows the remnant mass as a function of initial star mass. Fitting this semi-analytic estimate, and adding on the evolution of more massive stars, we develop some simple expressions of the fate of a Population III single star:

$$M_{\mathrm{fin}} = \begin{cases} 0.015M_{\mathrm{zams}}^2 - 0.199M_{\mathrm{zams}} + 1.491\ \mathrm{M}_\odot & 10 \leq M_{\mathrm{zams}} < 30.7\ \mathrm{M}_\odot & \mathrm{NS/BH} \\ -0.276M_{\mathrm{zams}}^2 + 22.69M_{\mathrm{zams}} - 426.4\ \mathrm{M}_\odot & 30.7 \leq M_{\mathrm{zams}} < 40\ \mathrm{M}_\odot & \mathrm{BH} \\ M_{\mathrm{zams}} & 40 \leq M_{\mathrm{zams}} < 100\ \mathrm{M}_\odot & \mathrm{BH} \\ M_{\mathrm{zams}} - f_{\mathrm{loss}}M_{\mathrm{env}} & 100 \leq M_{\mathrm{zams}} < 140\ \mathrm{M}_\odot & \mathrm{BH} \\ 0 & 140 \leq M_{\mathrm{zams}} < 260\ \mathrm{M}_\odot & \text{no remnant} \\ M_{\mathrm{zams}} & M_{\mathrm{zams}} \geq 260\ \mathrm{M}_\odot & \mathrm{BH} \end{cases} \quad (7)$$

where we adopt $f_{\mathrm{loss}} = 0.5$ for the fraction of the envelope lost by a star due to pulsational pair-instability. We also adopt $M_{\mathrm{max}}^{\mathrm{NS}} = 3\ \mathrm{M}_\odot$, the limiting mass below which we call remnant a neutron star, and over which BHs are formed. This translates into $M_{\mathrm{zams}} \sim 19\ \mathrm{M}_\odot$ for a minimum initial mass to form a BH. Stars with mass below 40 $\mathrm{M}_\odot$ lose part of their mass during the core collapse/supernova event. For higher masses, the collapse occurs with virtually no mass loss, and the entire pre-supernova star mass ends up in the final remnant.

There are two exceptions for high mass stars. In the range $100 \leq M_{\rm zams} < 140$ M$_\odot$ part of star's mass is removed through pulsational pair-instability and for $140 \leq M_{\rm zams} < 260$ M$_\odot$ the entire star is disrupted in pair instability supernova, with no remnant left.

Most of the massive stars do not lose much mass in the final evolutionary stages. However, if mass is lost, either through pulsational pair-instability or during core collapse and subsequent supernova explosion, the binary system may become eccentric. We assume spherical mass loss with no natal kick. We verify that the system is bound and then solve the Kepler equations for a new orbit.

2.3. Binary Interactions

Binary evolution may alter the final remnant mass of a given stellar component. During RLOF phases binary components may change their mass. If a donor star is a main sequence star, we assume that such configuration leads to the component merger and we terminate binary evolution. If a donor star is a giant, we assume that it looses its entire H-rich envelope in the ensuing RLOF. If a companion star accretes some of the donor material, it may either become rejuvenated (main sequence donors) or it simply increases its mass. Rejuvenation is performed with the increase of $M_{\rm zams}$ and recalculation of all star properties. When a giant star increases its mass, only its envelope mass is increased while the core remains unaffected.

The above mass transfer affects final masses of compact objects. If a star is rejuvenated, we use its new mass to calculate the final remnant mass (i.e., in eq. 7 new increased mass is used as $M_{\rm zams}$). In the case of mass loss, we assume that RLOF removes the entire H-rich envelope, and then pre-supernova mass is equal to the Helium core mass ($M_{\rm He}$). The final mass is then equal to either $M_{\rm He}$ or $M_{\rm fin}$, whichever number is smaller.

The binary orbit is allowed to change in the RLOF phases. Once a star overfills its Roche lobe, we check for dynamical stability of ensuing RLOF. If the mass ratio of the donor to the accretor is larger than $q_{\rm crit} = 2$, we assume evolution into common envelope (CE) phase. Otherwise, non-conservative, but dynamically stable, mass transfer (MT) is adopted. In both cases, the donor loses its entire envelope and becomes an exposed Helium core.

For the CE phase we use standard energy balance (Webbink 1984) and calculate the change of an orbit using:

$$\alpha_{\rm ce} \left(\frac{GM_{\rm don,f}M_{\rm acc}}{2a_{\rm f}} - \frac{GM_{\rm don,i}M_{\rm acc}}{2a_{\rm i}} \right) = \frac{GM_{\rm don,i}M_{\rm don,env}}{\lambda R_{\rm don,lob}} \tag{8}$$

where $M_{\rm don,env}$ is the mass of the donor envelope ejected from the binary, $R_{\rm don,lob}$ is the Roche

lobe radius of the donor at the onset of RLOF, and the indices i, f denote the initial and final values, respectively. In our calculations, we combine $\alpha_{\rm ce}$ (CE efficiency) and λ (the central concentration of the donor) into one CE parameter, and we assume that $\alpha_{\rm ce} \times \lambda = 1.0$. In the case of the CE phase it is assumed that no accretion on the companion takes place.

During dynamically stable MT episodes, part of the mass lost by the donor ($f_{\rm a}$) is accreted onto the companion, and the rest is lost from the system with a specific angular momentum equal to $2\pi j_{\rm mt} a^2/P$ (Podsiadlowski, Joss & Hsu 1992), where P denotes the orbital period. The change of orbit is calculated from

$$\frac{a_{\rm f}}{a_{\rm i}} = \frac{M_{\rm don,f} + M_{\rm acc,f}}{M_{\rm don,i} + M_{\rm acc,i}} \left(\frac{M_{\rm don,f}}{M_{\rm don,i}}\right)^{c_1} \left(\frac{M_{\rm acc,f}}{M_{\rm acc,i}}\right)^{c_2}, \tag{9}$$

where

$$c_1 \equiv 2j_{\rm mt}(1 - f_{\rm a}) - 2,$$
$$c_2 \equiv -\frac{2j_{\rm mt}}{f_{\rm a}}(1 - f_{\rm a}) - 2,$$
$$M_{\rm acc,f} = M_{\rm acc,i} + f_{\rm a}(M_{\rm don,i} - M_{\rm don,f}).$$

We assume that half of the mass lost from the donor is also lost from the system ($1-f_{\rm a} = 0.5$) with specific angular momentum $j_{\rm mt} = 1$, while the remaining half is accreted onto the companion.

2.4. Spin Evolution

Since the initial rotational velocities of Population III stars are unknown, we use two different assumptions for the initial spins. All the stars are initialized with rotational velocities

$$V_{\rm zams} = \begin{cases} 13.4 \times M_{\rm zams}^{-0.12}/(0.0389 + M_{\rm zams}^{-7.95}) & \text{moderate rotators} \\ 0.3 \times V_{\rm break} & \text{fast rotators} \end{cases} \tag{10}$$

where $M_{\rm zams}$ is expressed in $\rm M_\odot$, and $V_{\rm break} = \sqrt{GM_{\rm zams}/R_{\rm zams}}$ is the breakup (Keplerian) velocity at the star equator. In other words we have a model with fast rotating stars: 30% of the breakup velocity; and one in which we adopt a distribution of rotational velocities equal to those used in Population I stars. Population I initial velocities were taken from a fit presented in Belczynski et al. (2006; see § 2.3.3), which we extended to higher masses. In Figure 3 we show our assumptions on the initial velocities. We note that Population III stars (if initialized with $0.333 \times V_{\rm break}$) rotate much faster ($\sim 400 - 900$km s^{-1}) than Population I stars (~ 200km s^{-1}).

We then follow the evolution of the spin for each binary component. The spin angular momentum of a star can be written as

$$J_{\rm spin} = \begin{cases} k_{\rm ms} M R^2 \omega & \text{MS star} \\ k_{\rm env} M_{\rm env} R^2 \omega_{\rm env} + k_{\rm He} M_{\rm He} R_{\rm He}^2 \omega_{\rm He} & \text{giants} \\ k_{\rm He} M_{\rm He} R_{\rm He}^2 \omega & \text{He stars} \end{cases} \tag{11}$$

where M, R denote the mass and radius of an entire star, $M_{\rm He}$ is the He core mass and $M_{\rm env} = M - M_{\rm He}$ denotes the envelope mass, while $R_{\rm He}$ is the core mass. Spin of the entire star is marked with ω, while for the giants we denote the spin of He core and H envelope with $\omega_{\rm He}$ and $\omega_{\rm env}$, respectively.

Stage 1 During the main sequence, when no clear core-envelope structure exists, we assume uniform rotation of an entire star. Expansion on the main sequence (MS) slows down a star. Final angular velocity of a star on terminal MS is

$$\omega_{\rm tms} = (R_{\rm zams}/R_{\rm tms})^2 \; \omega_{\rm zams} \tag{12}$$

where $\omega_{\rm zams}$ is the angular velocity at ZAMS, and the radius at terminal MS is approximated with $R_{\rm tms} = 2.5 \; R_{\rm zams}$. Initial angular velocity of the entire star is thus reduced by a factor ~ 6.

Stage 2 Just after star leaves main sequence, the clear core-envelope structure appears. Initially core and envelope angular velocities are the same, and are obtained from the conservation of spin angular momentum while the star changes from a uniformly rotating MS star to a giant with core and envelope characterized by different moments of inertia

$$\omega_{\rm bgb} = \frac{k_{\rm ms} \; M \; R_{\rm tms}^2}{k_{\rm He} \; M_{\rm He} \; R_{\rm He}^2 + k_{\rm env} \; M_{\rm env} \; R_{\rm tms}^2} \; \omega_{\rm tms} \tag{13}$$

and then we set

$$\omega_{\rm env,bgb} = \omega_{\rm He,bgb} = \omega_{\rm bgb}. \tag{14}$$

This leads to a mild spin up of the core and envelope by factors of $\sim 1 - 1.5$ depending on its initial mass.

Stage 3 The rotation of the helium core will likely decouple from the envelope (end of main sequence/base of giant branch). However, it is not known how effective such decoupling might be. Therefore, during giant stage we follow the spins of the core and the envelope separately, allowing for partial core-envelope coupling. We introduce a simple spin He core–H envelope coupling to obtain

$$\begin{aligned} J_{\rm He,f} &= X_{\rm cou1} \; J_{\rm He,i} \\ J_{\rm env,f} &= J_{\rm env,i} + (1 - X_{\rm cou1}) \; J_{\rm He,i} \end{aligned} \tag{15}$$

where the indices i, f mark the angular momentum before and after the coupling, respectively. For simplicity we perform coupling in one step at the time just prior core collapse (end of star evolution) or prior to envelope loss for donors entering RLOF. The parameter $X_{\rm cou1}$ sets the strength of the coupling, and we calculate models with different values: 0.01 (strong coupling), 0.1 (weak), and 1.0 (none; core and envelope spins fully decoupled). As a result, He core is spun down, while envelope is spun up. The spin of a He core after coupling is

$$\omega_{\rm He,cou1} = X_{\rm cou1}\ \omega_{\rm He,bgb} \tag{16}$$

and it decreases by a factor of $1 - 100$ depending on the adopted value of $X_{\rm cou1}$. The new envelope spin (readily obtained from eq. 15) is not allowed to be larger than the new core spin; i.e., the core slows down only to the point at which the spins of the core and envelope are equal. Effectively, the final core spin may be in some cases larger than predicted by eq. 16 and is obtained from

$$\omega_{\rm He,cou1} = \frac{J_{\rm He,i} + J_{\rm env,i}}{k_{\rm He}\ M_{\rm He}\ R_{\rm He}^2 + k_{\rm env}\ M_{\rm env}\ R^2}. \tag{17}$$

Also, if rotation of the core is the same or slower than that of its envelope, the coupling is not performed. Such situations may occur in close binaries during the synchronization of the star.

Stage 4 Late in the evolution, the inner region of the He core condenses as it forms its iron core. We calculate the change of rotation in the inner $M_{\rm 7in} = 7$ M$_\odot$ conserving its angular momentum, i.e.,

$$\omega_{\rm 7in,Fe} = \frac{I_{\rm 7in,He}}{I_{\rm 7in,Fe}}\ \omega_{\rm He,cou1} \tag{18}$$

where $I_{\rm 7in,He}$, $I_{\rm 7in,Fe}$ denote moment of inertia of the inner 7 M$_\odot$ at the time of He core formation, and at the time of iron core formation, respectively. The inner region of the star compresses (see a drastic change of the moment of inertia; eq. 5- 6) and its angular velocity ($\omega_{\rm 7in,Fe}$) increases dramatically over its initial value ($\omega_{\rm He,cou1}$). The spin up factors are of the order of $\sim 3 - 100$ for stars with initial masses of $19 < M_{\rm zams} < 29$ M$_\odot$, and $\sim 100 - 1500$ for masses $29 < M_{\rm zams} < 500$ M$_\odot$.

Stage 5 We also perform a partial coupling of the inner 7 M$_\odot$ and the material surrounding it (the outer parts of He core; outside of inner 7 M$_\odot$) just prior to stellar collapse and remnant (and/or GRB) formation. Following from the conservation of spin angular momentum

$$\begin{aligned} J_{\rm 7in,f} &= X_{\rm cou2}\ J_{\rm 7in,i} \\ J_{\rm shell,f} &= J_{\rm shell,i} + (1 - X_{\rm cou2})\ J_{\rm 7in,i} \end{aligned} \tag{19}$$

we can obtain the final (prior the collapse) spin of the inner 7 M$_\odot$

$$\omega_{\rm 7in,col} = X_{\rm cou2}\ \omega_{\rm 7in,Fe} \tag{20}$$

where $J_{\rm shell}$, $J_{7\rm in}$ denote angular momentum of He shell and inner 7 $M_\odot$, respectively. We use $X_{\rm cou2}$ to set the strength of coupling, and we calculate models with different values: 0.01 (strong coupling), 0.1 (moderate coupling) and 1.0 (no coupling), adopted from Woosley & Heger (2006; see Table 1 for models with magnetic field coupling included and excluded). As a result, the inner parts are spun down by factors $\sim 1-10$. Magnetic torques were suggested as a mechanism responsible for such coupling (Spruit 2002). Note that, for massive stars, the iron core will be rotating faster (see eq. 18 and eqs. 5, 6) than its surrounding He shell. We assume that this is also the case if a star is subject to synchronization in a close binary. This is justified by the fact that while synchronization may work on a helium core for a prolonged time, once the iron core forms, it almost immediately collapses. We will relax this assumption in our parameter study.

Stage 6 Stages 1-5 cover spin evolution of a single star or non-interacting binary component. However, tidal interaction of stars in a short-period binary system may lead to an additional change of stellar spins. The strength of tidal synchronization/circularization for massive stars is not well constrained due to lack of observations. Therefore, we calculate two extreme models, one with and one without tidal interactions allowed. For the model with no tides the spin evolution of each binary component ends at stage 5. In the following we describe additional change of star spin due to the effect of tidal interactions.

Once a star fills a significant part of its Roche lobe we assume that tidal forces are strong enough to circularize the binary orbit and synchronize a given star. We use the criterion proposed by Portegies Zwart & Verbunt (1996)[2] to invoke circularization/synchronization

$$R_1 > 0.2a(1-e) \tag{21}$$

where a is semi-major axis of a binary orbit, e its eccentricity and R_1 is a radius of a binary component that is being synchronized. Orbital parameters (semi-major axis, spin of the synchronized star) change with conservation of the total angular momentum in the binary

$$J_{1,\rm spin} + J_{2,\rm spin} + J_{\rm orb} = const. \tag{22}$$

where the individual stellar components are marked with indices $i = 1,\ 2$, orbital angular momentum is calculated from $J_{\rm orb} = M_1 M_2 \sqrt{aG(M_1+M_2)(1-e^2)}/(M_1+M_2)$, while component spin angular momenta are taken from eq. 11 with current spin velocities (as calculated through stages 1-5). We solve eq. 22 for the new semi-major axis a requiring that the new orbit is circular ($e = 0$) and the star synchronized. Synchronization is obtained with

[2]The criterion was extended to include eccentric binaries; factor (1-e) was added to check for onset of tides at the closest (periastron) component encounter.

the condition

$$\begin{array}{ll} \omega_1 = \omega_{\rm tide} & \text{MS and He stars} \\ \omega_{1,env} = \omega_{1,He} = \omega_{\rm tide} & \text{giants} \end{array} \quad (23)$$

where $\omega_{\rm tide} = \sqrt{G(M_1 + M_2)}a^{-1.5}$ denotes the mean angular orbital velocity of the new synchronized binary, and index 1 marks the component that is being synchronized. The spin of the other component (2) is not affected. Note that we allow tides to work on an entire star (i.e., synchronization of both: envelope and core in case of giants). Stars at different evolutionary stages (MS stars, giants, naked He stars) are subject to synchronization provided that the condition 21 is fulfilled. Depending on the orbital separation of the system and the spin of the component that is being synchronized, tides may either increase[3] or decrease a star's angular velocity. We use population synthesis to determine the change of stellar spins due to tidal interactions.

2.5. Final Stages of Binary Evolution

If both the stellar components of the binary collapse to form compact objects (with or without accompanying GRB) without disrupting the binary, it will form a double compact object binary; most frequently a double black hole system. Such system will lose angular momentum through an emission of gravitational radiation, and will eventually merge, forming a single BH. This coalescence can produce a strong burst of gravitational radiation (Kulczycki et al. 2006).

The binary evolution may be additionally terminated either by the component mergers or binary disruption during supernova explosions. If a star on the main sequence initiates RLOF we always assume it leads to a merger, and single star formation. However, detailed evolutionary calculations of RLOF have yet to be performed for metal free stars to guide future population synthesis simulations. Additionally, we check for the component coalescence after any RLOF phase. If any stellar component radius is larger than its Roche lobe radius, a new single object is formed and we stop the evolution. It is noted that some of the merger products may be still potential GRB progenitors, but are not considered here, e.g. mergers of two exposed He-cores (Fryer, Hartmann, & Woosley 1999) or the merger of a compact remnant with a He-core companion (Fryer & Woosley 1998). We will analyze merger products as Population III GRB progenitors in a separate paper.

The binary may be disrupted because of the mass ejected in either the supernova (or GRB) explosion in the collapse of the stellar components or through mass loss caused by

[3]It is checked that a star is not spun up over breakup velocity.

pulsations[4]. The binary can also be disrupted if the stellar component undergoes a pair-instability explosion, leaving behind no remnant whatsoever. We assume that there are no natal kicks involved in the collapse/supernova of Population III stars. If Population III stars are subject to natal kicks, many Population III binaries are disrupted, terminating potential paths leading to a GRB phenomenon.

2.6. Initial Parameter Distributions/Standard Model

The initial mass function (IMF) of Population III stars is only known from numerical simulations (see O'Shea & Norman 2006 for most recent study). It is found to be top heavy and could be bimodal with a high mass peak around $100 M_{\odot}$ (Bromm et al. 1999, 2002; Omukai & Palla 2003) . The upper limit on the mass range is roughly $500\,M_{\odot}$ (Bromm & Loeb 2004). The lower limit is less certain and has been estimated to be $30\,M_{\odot}$ (Tan & McKee 2004), or $100\,M_{\odot}$ (Abel, Bryan & Norman 2002; Bromm & Larson 2004). The shape of the Population III mass function has been parametrized in different ways: a broken power law with $M_{break} = 100 M_{\odot}$, low mass slope of 0 and a high mass slope $2 < \beta < 3$ (Belczynski, Bulik & Rudak 2004), or a single power law with the Salpeter exponent (Bromm & Loeb 2006).

In our standard model we choose a mass range $10 - 500$ M$_{\odot}$. We draw a primary mass (M_1) from a power-law distribution $\Psi(M) \propto M^{-\beta}$ with $\beta = 2.35$ and within the adopted mass range. Next we draw a mass ratio ($q = M_2/M_1$) from flat distribution in range $q = 0-1$. If a secondary mass (M_1) is lower than the lower limit of the adopted mass range (10 M$_{\odot}$) we repeat the procedure, drawing primary mass and mass ratio again, until the secondary mass lies within the desired mass range. The resulting primary mass IMF is flat at low masses ($M_1 \lesssim 20$) and then falls off as a steepening power-law ($\sim M^{-1.8} - M^{-2.0}$). The resulting mass ratio is skewed toward high-q values. Both distributions are presented in Figure 4. An average mass of a primary is $M_{\rm av,1} = 44.8$ M$_{\odot}$, and secondary $M_{\rm av,1} = 27.4$ M$_{\odot}$. Therefore, average mass of a star in a binary system is $M_{\rm av,bin} = 36.1$ M$_{\odot}$, while a single star would have an average mass $M_{\rm av,sin} = 44.8$ M$_{\odot}$ (drawn from the same distribution as a primary star). The effect of a change of shape and mass range of IMF on the results is investigated in our parameter study.

The distribution of initial orbital separations is flat in logarithm like it is usually adopted for the Population I stars. Systems are allowed to form from the minimum separation, such that the stars are not in contact: $a_{\rm min} = 1.3\ R_{\rm 1,zams} + 1.3\ R_{\rm 2,zams}$, to maximum separation of

[4]Although in most cases, the entire pre-supernova star eventually ends up in the remnant (see eq. 7).

$a_{\rm max} = 10^6$ R$_\odot$. Initially all systems are placed on circular orbits. In each model calculation we evolve $N_{\rm bin} = 10^6$ primordial Population III binaries. We also adopt a binary fraction of $f_{\rm bin} = 0.1$ for Population III stars.

In addition, in our standard model, we use 30% of Keplerian velocity as initial star rotation speed, we allow tidal interactions (with tides working on an entire star), no natal kicks are applied at compact object formation, maximum NS mass is 3 M$_\odot$, CE efficiency is $\alpha_{\rm ce} \times \lambda = 1.0$, non-conservative evolution is applied during dynamically stable RLOF with $f_{\rm a} = 0.5$ and $j_{\rm mt} = 1$, coupling between He core and H-rich envelope is applied with $X_{\rm cou1} = 0.1$, and also coupling between Fe core and He shell is applied with $X_{\rm cou2} = 0.1$.

2.7. GRB Classification

We require that a star to make a GRB needs to: *(i)* lose its H-rich envelope and become a naked He star, *(ii)* the collapsing inner core must have a significant amount of angular momentum, *(iii)* and that the collapsing core forms a black hole remnant. Following evolution of each binary we easily select the stars that lose their envelopes and in the end form BHs. We also follow the evolution of the angular momentum in the star, obtaining an expression for the inner 7 M$_\odot$ core:

$$J_{\rm 7in} = I_{\rm 7in,Fe}\omega_{\rm 7in} \tag{24}$$

where $I_{\rm 7in,Fe}$ is given by eq. 6 and $\omega_{\rm 7in}$ is calculated from the spin evolution of each star in the simulation (see § 2.4). We also introduce the dimensionless specific angular momentum

$$\tilde{j}_{\rm 7in} = J_{\rm 7in}c/GM_{\rm 7in}^2 \tag{25}$$

where c is the speed of light, G gravitational constant, and $M_{\rm 7in}$ is the mass of the inner part of a collapsing core.

In order to form a disk around the newly formed black hole the specific angular momentum of the material must be large enough to prevent instant accretion. The specific angular momentum of a particle orbiting on the marginally stable orbit for a non-rotating black hole is $\tilde{j} = \sqrt{6}$. This condition (Podsiadlowski et al. 2004) was mentioned by Bromm & Loeb (2006), however, they did not verify if it is satisfied for their GRB progenitors originating from Population III binaries. Numerical simulations of a collapsing core (MacFadyen & Woosley 1999) showed that for the case of a 14 M$_\odot$ core a disk will form if the specific angular momentum before the collapse is in the range of $0.42 < \tilde{j} < 2.8$. For the core rotating too fast there was no significant accretion and a modest outflow took place. For each collapsing core in our simulations we calculate the value of its dimensionless specific angular

momentum $\tilde{j}_{7\rm in}$. The value $\tilde{j} = 1$ corresponds to the maximally rotating Kerr black hole. The requirement to make a GRB is that $\tilde{j}$ is close/larger than unity, and we consider three different potential ranges:

$$\begin{array}{ll} 0.42 < \tilde{j}_{7\rm in} < 2.8 & \text{MacFadyen \& Woosley (1999) (A)} \\ 1 < \tilde{j}_{7\rm in} < 10 & \text{this work (B)} \\ \tilde{j}_{7\rm in} > \sqrt{6} & \text{Podsiadlowski et al. (2004) (C)} \end{array} \quad (26)$$

where model (B) comes from the requirement that the newly formed black hole is spun fast enough to become maximally rotating Kerr black hole, and the accreting material has enough angular momentum to form a disk. As we will see below the particular choice of a given criterion A, B, or C does not change the results significantly.

2.8. SWIFT Detection Rates

We assume that the SWIFT detection threshold is $f_{\rm min} = 0.2 s^{-1}$ (Berger et al. 2005). The GRB luminosity function has been estimated by Sethi & Bhargavi (2001) who show that it can be well approximated by a lognormal distribution

$$\Phi(L) = \frac{e^{-\sigma^2/2}}{L_0\sqrt{2\pi\sigma^2}} \exp\left\{-\frac{[\ln(L/L_0)]^2}{2\sigma^2}\right\} \quad (27)$$

centered on $L_0 = 2 \times 10^{56} s^{-1}$, with a width of $\sigma = 2$. We can now easily find the GRB rate by integrating:

$$R_{SWIFT} = \frac{\eta_{mass}\eta_{beam}\eta_S\eta_i}{M_{av,bin}} \int \Phi(L) dL \int_0^{z_{max}(L)} \frac{SFR(z)}{1+z}\frac{dV}{dz} dz \quad (28)$$

where η_{beam} is the beaming correction, η_S is the SWIFT GRB detection efficiency, $\Psi(L)$ is the luminosity function, and $SFR(z)$ is the Population III star formation rate. The GRB formation efficiency η_i is the number fraction of stars in Population III binaries that make GRBs (see eq. 34).

The fraction of entire Population III mass that is contained in the binaries is denoted as η_{mass}. We define binary fraction as $f_{\rm bin} = N_{\rm bin}/(N_{\rm bin} + N_{\rm sin})$, where $N_{\rm bin}$ and $N_{\rm sin}$ denote the number of binary and single stars in a given population, respectively. If so, then the mass fraction is

$$\eta_{mass} = \frac{2 f_{\rm bin} M_{av,bin}}{2 f_{\rm bin} M_{av,bin} + (1 - f_{\rm bin}) M_{av,sin}} \quad (29)$$

where $M_{av,bin}$ denotes the average star mass in a binary system, while $M_{av,sin}$ is an average mass of a single star, both of which depend on adopted IMF. For the standard model IMF,

we have $M_{av,bin} = 36\,M_\odot$ and $M_{av,sin} = 45\,M_\odot$, and then for the adopted binary fraction $f_{\rm bin} = 0.1$ we obtain $\eta_{mass} = 0.15$.

The limiting redshift is obtained by solving

$$d_l(z_{max})(1+z_{max})^{(\alpha-2)/2} = \sqrt{\frac{L}{4\pi f_{min}}} \tag{30}$$

where $d_l(z)$ is the luminosity distance, and α is the photon index of the GRB spectrum. We assume that $\alpha = 2$. The Population III star formation rate is poorly known therefore we will parametrize its shape by box function:

$$SFR(z) = S\Theta(z - z_{start})\Theta(z_{stop} - z) \tag{31}$$

where $\Theta(z)$ is the Heaviside function. With this choice equation 28 can be simplified to

$$R_{SWIFT} = 3{\rm yr}^{-1}\eta_i \left(\frac{\eta_{mass}}{0.15}\right)\left(\frac{\eta_{beam}}{0.02}\right)\left(\frac{\eta_S}{0.1}\right)\left(\frac{S}{S_0}\right)\left(\frac{36M_\odot}{M_{av}}\right)\left(\frac{F(z_{start}) - F(z_{stop})}{3.93}\right) \tag{32}$$

where $S_0 = 10^{-2}M_\odot{\rm Mpc}^{-3}$ and $F(z)$ is

$$F(z) = (10^7{\rm Mpc}^3)^{-1}\int \Phi(L)dL \int_0^{z_{max}(L)} \frac{\Theta(z-z')}{1+z'}\frac{dV}{dz}dz'\,. \tag{33}$$

The typical values of the rightmost factor in equation 32, $(F(z_{start}) - F(z_{stop}))$, lie in the range between one and ten. Thus the rate is directly proportional to η_i – the GRB production efficiency, which is obtained with evolutionary calculations of Population III binaries. If GRB production from Population III binaries is very efficient, one can expect a few events detectable by SWIFT per year.

3. Results

In the following subsections we first present results for our standard evolutionary model (see § 2.6), and then show the sensitivity of results on a number of adopted parameters. For the sake of presentation, we will consider "*potential GRB progenitors*" defined as stars that are stripped of their H-rich envelopes and are massive enough to form BH (but no constrains are put on their specific angular momentum) and "*GRB progenitors*" for which we additionally apply angular momentum constraints (see eq. 26).

3.1. Evolutionary Scenarios

We consider a number of evolutionary channels to form potential GRB progenitors in Population III binaries. The major channels are presented in Table 1. GRB progenitors evolve through RLOF by either dynamically stable MT or dynamically unstable CE phases, which expose the He cores of the stellar component/components. A star initiating a given event is indicated with a number: 1 stands for primary (initially more massive star) and 2 for secondary binary component. By potential progenitor we consider any star that has been stripped of its H-rich envelope that will form BH. Only $\sim 10\%$ of stars in Population III binaries end up as exposed He cores massive enough to form BH. In particular it is found that in some cases both the primary and secondary components are stripped of their H-envelopes and may produce a potential GRB. The most efficient channel (grb01) involves both MT and CE episode and $\sim 7\%$ binaries. However, if constraints on the angular momentum are imposed (see eq. 26) only small fraction of binaries forms cores with high angular momentum to produce GRB. Table 1 lists formation efficiencies along each channel for different constraints on angular momentum. The formation efficiency (per star in Population III binary) is defined as

$$\eta_i = \frac{N_{\rm grb}}{2N_{\rm bin}} \tag{34}$$

where $N_{\rm bin} = 10^6$ is the total number of binaries evolved in a given simulation, $N_{\rm grb}$ the number of stars that have produced a GRB, and i denotes angular momentum constrain used: in case of no angular momentum constraints (η_1); MacFadyen & Woosley 1999 (η_2); this work (η_3); and Podsiadlowski et al. 2004 (η_4). It is found that if angular momentum constraints are imposed, GRBs are found to be formed only through the grb01 channel. In particular, only a small fraction of secondaries formed through channel grb01 have sufficiently high angular momentum to produce a GRB. Formation efficiencies are very small, $\eta_2 = 0.0002$, $\eta_3 = 0.0058$, $\eta_4 = 0.0063$ due to very specific conditions required to form a fast rotating core of a massive star in Population III binary. In the following we give a brief description of a sample evolution of a progenitor system (channel grb01) leading to the formation of a GRB.

We take an example of an initial binary consisting of a $M_1 = 40$ M$_\odot$ primary and $M_2 = 31$ M$_\odot$ secondary on an orbit with a semi-major axis of $a = 75$ R$_\odot$ (orbital period $P_{\rm orb} = 8.9$ day). The maximum radii are 161 and 44 R$_\odot$ for the primary and secondary components, respectively. Since their Roche lobes are only ~ 30 and 27 R$_\odot$ the system is bound to evolve through two RLOF episodes. Stars are initiated with the uniform angular rotation velocities of $\omega_1 = 23.1$ day^{-1} and $\omega_2 = 28.8$ day^{-1}.

As the primary expands onto the giant branch, it synchronizes as it fills its Roche

lobe; its envelope spins up while core slows down to and angular velocity (ω_1) equal to $2\pi/P_{\rm orb} = 0.7$ day^{-1}. Since the core and envelope are spinning at the same rate there is no coupling (angular momentum transport from core to envelope) performed in this case. Change of the primary spin is done at the cost of orbital angular momentum and the orbit decays to $a = 72$ R$_\odot$ ($P_{\rm orb} = 8.5$ day). The first mass-transfer episode is dynamically stable (comparable component masses) and the orbit tightens only moderately $a = 42$ R$_\odot$ ($P_{\rm orb} = 4.1$ day). The primary loses its envelope and becomes a naked He star ($M_1 = 13$ M$_\odot$), while the secondary accretes a fraction of the mass and is rejuvenated ($M_2 = 45$ M$_\odot$). Now we check if the He star primary (radius of $R_1 = 0.3$ R$_\odot$) fills a significant part of its Roche lobe to undergo further synchronization. Since this is not the case ($R_1 \ll a$), the He star spin remains unchanged ($\omega_1 = 0.7$ day^{-1}). Then the inner core compresses, and we spin it up to from $\omega_1 = 0.7$ day^{-1} to $\omega_1 = 594$ day^{-1} to take into account the 3 order of magnitude decrease of the moment of inertia of the inner parts of the He core. Just before the collapse we perform the coupling, and the inner core loses a fraction of its angular momentum ($X_{\rm cou2} = 0.1$) to the surrounding He material, and it slows down to $\omega_1 = 59.4$ day^{-1}. In this mass range the star forms a BH with no mass loss ($M_1, BH = 13$ M$_\odot$). As the star collapses the specific angular momentum of the inner part of the collapsing star is only $\tilde{j} \sim 0.02$, and the star does not produce a GRB due to insufficient angular momentum. After SN the orbit remains bound and unaffected (no mass loss, no natal kick).

Then the secondary evolves off its main sequence ($\omega_2 = 3.5$ day^{-1}), and while climbing up the giant branch and filling its Roche lobe, it synchronizes to $\omega_2 = 1.8$ day^{-1}. Coupling between He core and H envelope is not performed since both rotate with the same angular velocities. The secondary initiates a second RLOF episode at $a = 37$ ($P_{\rm orb} = 3.4$ day). Because the donor ($M_2 = 45$ M$_\odot$) is now much more massive than its BH companion ($M_{1,\rm BH} = 13$ M$_\odot$) the following RLOF is dynamically unstable and the system enters CE phase. The orbit tightens significantly to $a = 1.2$ R$_\odot$ ($P_{\rm orb} = 0.029$ day), the secondary loses its envelope and becomes an exposed helium core ($M_2 = 14.8$ M$_\odot$). Since the post-CE orbit is so small, the Helium star ($R_1 = 0.3$ R$_\odot$) fills a significant part of its orbit ($R_1 > 0.2a$) and synchronizes. After synchronization, the star is rapidly spinning ($\omega_2 = 250$ day^{-1}) and the orbit tightens slightly to $a = 1.1$ R$_\odot$ ($P_{\rm orb} = 0.025$ day). When the core condenses during oxygen and silicon burning, it is spun up to $\omega_1 = 221100$ day^{-1} through decrease of moment of inertia of the material forming it. Finally, we perform coupling of the Fe core with He shell ($X_{\rm cou2} = 0.1$), spinning the inner core down to $\omega_1 = 22110$ day^{-1}. Fast rotation of the inner core results in a large specific angular momentum of the secondary at the time of the collapse, $\tilde{j}_2 \sim 6$. Depending on the angular momentum criterion, the secondary may (B, C) or may not (A) produce a GRB. The secondary after the collapse forms BH with mass $M_1, BH = 14.8$ M$_\odot$. The close massive BH-BH binary forms with $a = 1.1$ R$_\odot$ ($P_{\rm orb} = 0.025$

day) and its components merge due to the emission of GR in less than 0.1 Myr.

3.2. Effects of Tides

At every step the population synthesis code takes a new semi-major axis a and subsequently new stellar spin $\omega_{\rm tide}$ is established. The change of the core angular velocity due (only) to the tidal effects is calculated as

$$d_{\rm cor,vel} = \frac{\omega_{1,\rm f}}{\omega_{1,\rm i}} \tag{35}$$

where $\omega_{1,\rm i}$ denotes the initial (pre-synchronization) velocity of He core, and $\omega_{1,\rm f} = \omega_{\rm tide}$ is the post-synchronization velocity.

The effects of tides on core angular velocity are presented in Figure 5. For our reference model we have recorded change of the core rotational velocity ($d_{\rm cor,vel}$) for primaries and secondaries. Only $\sim 25\%$ primaries, and $\sim 5\%$ secondaries are subject to synchronization, as systems are disrupted in SNa explosions, binary components merge in RLOF events, or some systems are simply too wide to interact.

In most cases the tides are effective when a star is already on the giant branch, and has a large (as compared to the orbit size) radius. By that time, the core has decoupled from the envelope; and its spin is much larger than that of an expanding envelope. Generally, once tides become effective, the mean orbital angular velocity is smaller than the core angular velocity, and the subsequent synchronization slows down the stellar core. For cores which are affected by tides during the giant branch, the speed decreases by factors of $\sim 1 - 1000$ ($d_{\rm cor,vel} \sim 1 - 0.001$). However, we find a subpopulation of secondary cores with a rather high tidal speed-up factors $d_{\rm cor,vel} \sim 30 - 100$. In some cases, a naked Helium star is subject to synchronization. This happens only for small orbits since the radii of Helium stars are rather small (< 2 R$_\odot$; see eq. 3). Such configuration is encountered in the late evolutionary stages of a massive binary. After the primary has already formed a compact object, the secondary may initiate a common envelope phase, that leads to a drastic orbital tightening. As a result, a short period binary with secondary He star emerges. If the orbit is sufficiently small, tides are operating and the He star is synchronized. Since the mean orbital angular velocity is then rather large, the Helium star can spin up significantly.

In Figure 6 we show the final specific angular momentum of the inner core for our reference model. For single stars (that are in the mass range to form black holes) we find $\tilde{j}_{\rm 7in} \sim 0.01 - 0.02$ which is a direct result of the adopted single stellar models (§ 2.1) and assumptions stated in § 2.4. Primary stars are characterized by $\tilde{j}_{\rm 7in} \sim 10^{-4} - 0.1$. The low

values $\tilde{j}_{7\mathrm{in}} < 0.01$ are the result of tidal spin down on giant branch. The high values $\tilde{j}_{7\mathrm{in}} > 0.02$ are a combination of the synchronization without spin down (see Figure 5; not all of the cores are significantly slowed down) that leads to a lack of angular momentum transport since the core rotates with the same angular velocity as envelope. Secondary stars show a bimodal distribution of the core specific angular momentum. Low values $\tilde{j}_{7\mathrm{in}} \sim 10^{-3} - 0.1$ are found for secondaries that were spun down during giant branch, while high values $\tilde{j}_{7\mathrm{in}} \sim 2 - 10$ are found for secondaries that were spun up as a naked Helium stars. Only for this last subpopulation is the specific angular momentum high enough to warrant a potential GRB.

3.3. Properties of GRB Progenitors

In Figure 7 and 8 we present the initial (ZAMS) masses of potential GRB progenitors and the BH masses they form, respectively. The initial mass distribution spans almost the entire investigated mass range $M_{\mathrm{zams}} = 10 - 500$ M$_\odot$. However, primaries only over $M_{\mathrm{zams}} \gtrsim 19$ M$_\odot$ may form BHs (and only such stars are included as potential GRB progenitors). There are no primaries in the initial mass range $140 - 260$ M$_\odot$ because such stars become pair instability supernovae. For secondaries the range is narrower $\sim 140 - 180$ M$_\odot$ due to rejuvenation, and in particular stars over ~ 180 M$_\odot$ may gain enough mass ($\gtrsim 80$ M$_\odot$; half of the primary envelope) to be shifted out of pair instability supernovae mass strip.

Black holes are found within mass range $\sim 3 - 250$ and $\sim 3 - 320$ M$_\odot$ for primary and secondary components, respectively. The low-mass cut reflects our assumption on the minimum BH mass, and the high-mass cut corresponds to He core mass of the most massive star in the simulation; $M_{\mathrm{He}} = 250$ M$_\odot$ ($M_{\mathrm{zams}} = 500$ M$_\odot$) for primaries, and $M_{\mathrm{He}} = 320$ M$_\odot$ ($M_{\mathrm{zams}} = 630$ M$_\odot$) for rejuvenated secondaries. Pair instability supernova prevent the formation of BHs in secondaries within the mass range between ~ 60 and 120 M$_\odot$. Here, the empty interval is the same for both components. The stripped primaries (potential GRB progenitors included here) just outside of pair instability range form BHs with masses 60 ($M_{\mathrm{zams}} = 140$) and 120 M$_\odot$ ($M_{\mathrm{zams}} = 260$ M$_\odot$). Secondaries with initial masses that fall within pair instability supernova mass range ($M_{\mathrm{zams}} \sim 180 - 260$ M$_\odot$) gain enough mass and are rejuvenated to form BHs as stars with $M_{\mathrm{zams}} > 260$ M$_\odot$. The remaining part of the BH mass distribution follows directly from the initial mass function and envelope removal through RLOF.

Additionally, we separately show these progenitors (and the corresponding BHs) that will attain enough specific angular momentum ($\tilde{j} \gtrsim 1$) to produce a GRB. As mentioned before, it is found that only secondaries form such high rotating cores. Both distributions for this subpopulation, follow closely their counterparts for potential GRB progenitors. Since

only a small fraction of secondaries gain high speeds and high specific angular momenta, the numbers are much smaller for potential progenitors. The majority of Population III collapsars ($\sim 98\%$) are formed from the lower mass end of the population III stars ($M_{\rm zams} \sim 10 - 100$ M$_\odot$), and could be similar to Population I and II collapsars. Only a small subset of collapsars ($\sim 2\%$) originate from very massive stars ($M_{\rm zams} \sim 200 - 500$ M$_\odot$) since such massive stars are hard to be accommodated in binaries small enough that the synchronization would provide enough angular momentum to produce a GRB.

3.4. Parameter Study

Results of alternative evolutionary models are presented in Table 2. In the following we discuss the effect of various parameters on our results.

If the tides are only allowed to work on the envelope of the extended star (giants with clear core and envelope structure) and not on its core (Mod05), the results remain unchanged. Since tides are the only effectively spinning naked He stars in close (post-CE) binaries, the tidal interactions prior to that stage do not play an important role in producing GRBs. Had we not allowed tidal interactions to be effective for naked He stars, then the situation changes and of course we then do not produce any GRBs. It is seen in a general case in which we do not allow any tidal interactions (Mod02); no GRBs are formed, but almost the same number of potential progenitors is found. Simply the stars are not spinning fast enough (no tidal spin up) to satisfy any of specific angular momentum criteria we have imposed.

We have assumed in our modeling that there is no angular momentum accretion in RLOF events. That it is most probably not the case as the accreted mass carries its own non-zero angular momentum. If angular momentum is transferred from one component to the other with mass, it may alter the spin of the components. We have calculated a model (Mod14) in which we have allowed accreting stars to maximally increase their rotational velocities (to Keplerian velocity). This happens during stable RLOF (prolonged phase, mass accretion) when the evolved primary transfers mass to the main sequence secondary. Main sequence stars are assumed to rotate uniformly, and the entire star is spun up. However, such a spin up has no effect on the predicted GRB formation efficiencies. This is due to a simple fact that all GRB progenitors are subject to tidal synchronization that sets the star speed in later evolutionary stages. Therefore, no matter how much the star was spun up in early evolutionary stages, once it is subject to tidal interactions it will be slowed down to the speed set by the size of its orbit. We do not follow the corresponding spin down of the donors. Had it was included it would not have altered the GRB formation efficiencies, since the GRB progenitors originate from fast rotating helium cores that were spun up by

synchronization in close binaries after mass transfer episodes were over.

If we impose natal kicks for all compact objects (Mod03), some binaries are disrupted and the GRB formation efficiencies ($\eta_{\rm i}$) decrease to 60-80% of the standard model values. Although we have used quite large kicks drawn from Maxwellian distribution with $\sigma = 265$ km s^{-1} (Hobbs et al 2006; the most recent estimate for Population I stars), there is only a rather small decrease in formation efficiency of GRBs. Once we impose kicks many binaries are disrupted in SNe explosions. However, the GRB progenitors evolve through one or two RLOF episodes and are found on close orbits and therefore are hard to disrupt.

The change of the minimum mass of a Population III star from 10 to 30 M$_\odot$ (Mod04) increases the GRB formation efficiencies by factor of ~ 3. This is due to the fact that we assume that stars with $M_{\rm zams} < 19$ M$_\odot$ form NSs instead of BHs (unless these stars accrete mass) and increasing of initial mass over the BH formation threshold enhances the chances of forming a GRB progenitor. The average stellar mass in the simulation increases to $M_{\rm av,bin} \sim 88$ M$_\odot$, and it is ~ 2.5 larger than in the standard model, therefore the GRB detection rate remains basically unaffected as the two factors cancel out (see eq. 28). Since the binary fraction is the same as in the standard model, the mass fraction $\eta_{\rm mass}$ does not change either ($M_{\rm av,sin} \sim 105$ M$_\odot$ for this model).

We performed one calculation (Mod13) performed using our "moderate rotator" prescription for rotation speeds (see eq. 10). The stars are initialized with speeds that are characteristic of Population I stars (~ 200 km s^{-1}). GRB formation efficiencies does not change substantially, since the final spin up for He cores making GRB progenitors does not depend on the star initial spin, but rather on the size of the orbit of binary undergoing synchronization.

We also perform a calculation with the alternative IMF for Population III stars (Mod12); both component masses are drawn independently from a power-law distribution with $\beta = -2.35$ within the same mass range as in the standard model ($10 - 500$ M$_\odot$). The resulting distribution of mass ratio, defined now as mass ratio of the less massive component to the mass of the more massive component), is flatter than in the standard model (see Figure 4). The average mass of a star in binary and a single star is now the same and is $M_{\rm av,bin} = M_{\rm av,sin} = 28.9$ M$_\odot$, and we obtain $\eta_{\rm mass} = 0.18$. GRB formation efficiencies drop by factor of ~ 2 in this model, however due to the lower average star mass in this simulation, the *SWIFT* detection rates are not greatly affected (change by factor of ~ 0.75).

Maximum increase of binary fraction (to $f_{\rm bin} = 1$) may increase the *SWIFT* detection rate by factor of ~ 7 (see eq. 29). However, such a high binary fraction in Population III seems very unlikely due to the fact that primordial gas was much harder to fragment than

metal-rich gas of Population I and in particular binaries may have not formed at all (e.g., Ripamonti & Abel 2004).

We have also investigated the influence of adopted CE efficiency on our results. With the decreased CE efficiency ($\alpha_{\rm ce} \times \lambda = 0.3$; Mod10) the GRB formation efficiencies change by factors ~ 0.7, while with the increased CE efficiency ($\alpha_{\rm ce} \times \lambda = 3$; Mod11) they change by factors ~ 1.3. Change of CE efficiency has an important role on the post-CE orbital separation of a binary system. That in turn plays a crucial role for systems that are GRB progenitors (components need to be close enough for tides to spin up naked He core of the secondary). If post-CE orbit is too wide, He core is not spun up enough to form a GRB, and if post-CE orbit is too tight, the binary components merge. The CE acts as a simple orbital separation filtering, and changing the CE efficiency allows CE to send different pre-CE binaries to the given post-CE separation range. Therefore, as long as there is a wide range of pre-CE separations, change of the CE efficiency will only select different binaries to fall within specific required post-CE orbit range (required, e.g., for GRB formation).

Coupling of the He core with H envelope during giant phase is not important for the formation of GRBs. Models with strong coupling ($X_{\rm cou1} = 0.01$; Mod06) as well as with fully decoupled He cores ($X_{\rm cou1} = 1$; Mod07) generate the same numbers of GRBs. Since the GRB progenitors are synchronous at giant stage (close binaries) their cores rotate at the same speed as envelopes, and therefore cores does not loose any angular momentum in the process.

In case of a very strong coupling of iron core to the surrounding He shell ($X_{\rm cou2} = 0.01$; Mod09) the collapsing cores has 10 times less specific angular momentum then in the standard model, and the GRB formation efficiencies change: $\eta_2 = 0.0053$, $\eta_3 = 0.0006$, $\eta_4 = 0.0$ (η_1 is unchanged since the similar potential progenitors are formed). Still the same population of synchronized secondary helium stars make GRB progenitors. We note the significant increase (factor ~ 25) in η_2, although the efficiency is still relatively small.

If we assume that an iron core is not coupled to the surrounding He shell ($X_{\rm cou2} = 1$; Mod08) then the core doesn't lose angular momentum and is spinning fast. The specific angular momentum in this model is presented in Figure 9. Since specific angular momentum is proportional to iron core speed, and the speed is higher by factor of 10 than in standard model, now both primaries and secondaries can produce a GRB. The subpopulation of secondary helium cores that are spun up through tidal interactions and that are the sole GRB progenitors in other models may in this evolutionary scenario have specific angular momenta that are too high to produce a GRB ($20 < \tilde{j} < 150$). The GRB formation efficiencies are following: $\eta_1 = 0.1041$, $\eta_2 = 0.0242$, $\eta_3 = 0.0111$, $\eta_4 = 0.0067$. As compared to standard model, η_1 does not change since it includes all potential GRB progenitors (no

constraint on specific angular momentum), also η_4 is not affected too much as it includes only very high angular momentum systems (synchronized helium stars as in standard model), and the additional stars don't make the cut (see Figure 9). The highest increase (two orders of magnitude) is observed for η_2 as it encompasses the largest fraction of additional fast spinning cores (mostly originating from primaries), and the moderate increase is found for η_3 which is doubled. Note that the subpopulation of stars making GRBs in the standard model, does not contribute to η_2 nor η_3 due to their very high specific angular momentum. These are the highest GRB formation efficiencies that we obtain within our modeling.

Although this assumption (no angular momentum loss from the inner core) may be contrary to the expectations for single stars (Spruit 2002; Woosley & Heger 2006) it may potentially work for some stars in close binaries. For binary components that are subject to strong tidal interactions, that may make the entire star rotate synchronously, the iron core included. If this is the case, the stars that go through synchronization are not subject to angular momentum transport (uniform rotation) and then results of this model should be considered as representative of binary population. With the lack of observational evidence on the effectiveness of tides and also lack of theoretical work for Population III stars, we treat this as a major uncertainty of our binary evolutionary model.

3.5. Population III GRB Detectability

Population III stars evolve very quickly so their redshift distribution follows the star formation rate. For simplicity we assume that Population III stars were formed between redshifts 10 and 30 and that the star formation rate is in this epoch was $S = 10^{-2} M_{\odot}\mathrm{Mpc}^{-3}$. For the calculation of the rate this is an optimistic assumption since the actual redshift range for Population III stars is probably smaller. For this choice of redshifts, we obtain $F(30) - F(10) = 3.93$. The GRB formation efficiencies are listed in Table 2 and we can use equation 32 to calculate SWIFT detection rate. We obtain $\sim 0.001 - 0.02\mathrm{yr}^{-1}$ for standard model calculation, range resulting from the different constrains on specific angular momentum used. Even for the model with no angular momentum loss for iron cores, for which we find the highest GRB formation efficiency ($\eta_2 = 0.0242$) *SWIFT* detection rate goes only up to $\sim 0.1\mathrm{yr}^{-1}$.

This result has been obtained with rather conservative assumptions. We have chosen a large binary fraction ($f_b in = 0.1$) for Population III and a rather wide beaming fraction corresponding to the typical beaming half angle of 11 degrees. We have also chosen a rather large value of the redshift range in which Population III stars are formed. The star formation rate we have used can not be increased by much as well. Thus we consider our estimate as a

very safe upper limit estimate for collapsars from the Population III binaries observable by SWIFT.

4. Discussion

We have modeled the evolution of Population III binaries using the most up to date numerical models of such stars. By focusing on binary progenitors that both eject the hydrogen envelope and spin up the core prior to collapse, we estimate the fraction of these systems that produce potential GRB progenitors. We find that the typical scenario to form such a star produces GRBs from the star that is, at least initially, less massive. It was found that significant fraction of stars ~ 0.1 lose their H-rich envelopes through binary interactions and are massive enough to form BH. However, only a small fraction of stars ~ 0.01 have been additionally spun up by tidal interactions to a sufficient specific angular momentum to make a GRB. Majority ($\sim 98\%$) of the collapsing cores that make GRBs have relatively low masses and are in the range $\sim 5 - 50$ $M_{\odot}$, and only a very few Population III collapsars are produce from massive cores $\sim 150 - 300$ $M_{\odot}$.

We calculate the expected detection rate of Population III GRBs by SWIFT and find that it is very low, $\sim 0.001 - 0.02 \mathrm{yr}^{-1}$ for our standard evolutionary model. Even for the most optimistic model, in which we do not allow angular momentum loss from the collapsing core, the rate is rather low $\sim 0.1 \mathrm{yr}^{-1}$. There are two main reasons for this. First, the overall potential detection rate from Population III binaries is relatively small. Even if we assume that all stars in Population III binaries make a GRB, we would expect only $\sim 3 \mathrm{yr}^{-1}$, and this only under optimistic assumptions on binary fraction and GRB collimation. Second, it is difficult to spin the stars up through tidal interactions, sufficiently enough to make a GRB. Only a small fraction of stars in binaries (~ 0.01) are subject to such a strong spin up. Bromm & Loeb (2006) assumed that all the exposed He cores are spun up sufficiently to make a GRB. This assumption led to an overestimate of high redshift GRBs. In contrast, we find that there should be no detectable high redshift GRBs from Population III binaries. This conclusion only weakly depends on a number of evolutionary unknowns. If, however, high redshift bursts are detected and are identified with Population III stars, then our results argue against this particular collapsar progenitor scenario for such bursts. One should note that the expected rate of gravitational wave bursts from coalescences of double black hole binaries originating in Population III stars in the advanced LIGO is a much more promising way to investigate the properties of Population III binaries (Belczynski et al. 2004; Kulczycki et al. 2006).

The collapsar scenario requires that the star is stripped of its outer layers in order for the

jet to be able to break out. In the above models we only consider stars stripped of hydrogen envelopes, however some scenarios, and some observations, also require the removal of most of the helium envelope. At this stage the models are not advanced enough to investigate this scenario in detail. However, we have estimated the number of helium stars that fill the Roche lobes and hence may potentially be stripped of their He-rich envelopes. Only a small fraction of stars ($\lesssim 0.05$) in Population III binaries may lose their He-rich envelopes and even if all of them are spun up enough to produce GRBs the resulting rate is then only $\sim 0.15\mathrm{yr}^{-1}$. One notable difference is that in this case most of the bursts would come from the initially more massive star (Star 1). Further analysis, once better models of Population III stars are available, should allow to investigate this issue. Also, a component merger, a new single star, may be spinning much faster than the original components, and provide enough angular momentum to make GRB. Such mergers are encountered in binary evolution during RLOF phases. Although we do not follow the evolution of such merger products, their formation rate is also rather small; only about ~ 0.05 stars in Population III binaries merge before forming compact remnants, resulting again in a rather small SWIFT detection rate of $\sim 0.15\mathrm{yr}^{-1}$. Another possibility of forming GRB in a binary is a common envelope merger of a giant and a main sequence star (Ivanova et al. in preparation; Podsiadlowski 2006, GRB symposium in London). The inspiralling main sequence star supplies pure hydrogen to the He burning shell of a giant, the resulting flash removes the envelope of a giant. Also the in falling hydrogen-rich material may spin up the Helium core of a giant. Although details of the model has not been worked out in case of zero metallicity Population III stars, we have estimated number of potential common envelope configurations. Such common envelope mergers are found more frequently ~ 0.017 than the GRBs formed through tidal spin up (see Table 2) but are still not numerous enough to warrant *SWIFT* detection ($\sim 0.05\mathrm{yr}^{-1}$), even if we assume that all such events lead to a GRB (overestimate, since only very specific initial conditions of an inspiral and stellar structure of binary components may lead to a GRB; Ivanova, private communication).

We do not find enough GRB progenitors in Population III binaries to warrant detection with *SWIFT*. If binaries exist in Population III at all, they may provide potential gravitational radiation signature, through mergers of their end products: massive double black holes (see e.g., Kulczycki et al. 2006). If GRBs are detected, an ideal candidate might be the single star, high-mixing models proposed by Yoon & Langer (2005; see also Woosley & Heger 2006). Although this progenitor is unlikely to be the primary progenitor for GRBs at low redshift (Fryer 2006b), it could make a considerable contribution to the GRB population at high redshift. If all the stars were single in Population III, and if we have assumed that *all* of them produce a GRB, we would obtain *SWIFT* detection rate of $\sim 18\ \mathrm{yr}^{-1}$ (see eq. 32, with $\eta_i = 1$ and $\eta_{\mathrm{mass}} = 1$). However, during about 2 years of *SWIFT* observations there was

no detection of an extreme redshift ($z > 10$) GRB. This, in principle, could put an upper limit on the Population III single star GRB model.

We acknowledge the support of KBN grant 1P03D02228, and KB thanks Kasia Samson (Warsaw University) for help on this manuscript. Also we would like to thank T.Abel, W.Dziembowski and B.O'Shea for comments on initial spins and parameters of Population III stars. Support for CLF and AH was carried out under the auspices of the National Nuclear Security Administration of the U.S. Department of Energy at Los Alamos National Laboratory under Contract No. DE-AC52-06NA25396 and funded, in part, by a NASA Grant SWIF03-0047, by the National Science Foundation under Grant PHY99-07949 and by the DOE Program for Scientific Discovery through Advanced Computing (SciDAC; DE-FC02-01ER41176).

REFERENCES

Abel, T., Bryan, G.L., & Norman, M.L. 2002, Science, 295, 93

Belczynski, K., Bulik, T., Rudak, B. 2004, ApJ, 608, L45

Belczynski, K., Kalogera, V., & Bulik, T., 2002, ApJ, 572, 407

Belczynski, K., et al. 2006, ApJS, submitted (astro-ph/0511811)

Baraffe, I., Heger, A., & Woosley, S.E. 2001, ApJ, 550, 890

Berger, E., et al. 2005, ApJ, 634, 501

Bond, J.R., Arnett, W.D., & Carr, B.J. 1984, ApJ, 280, 825

Bromm, V., Coppi, P.S., & Larson, R.B. 1999, ApJ, 527, L5

Bromm, V., Coppi, P.S., & Larson, R.B. 2002, ApJ, 564, 23

Bromm, V., & Larson, R.B. 2004, ARA&A, 42, 79

Bromm, V., & Loeb, A. 2006, ApJ, submitted (astro-ph/0509303)

Cen, R. 2003, ApJ, 591, 12

Chabrier, G. 2003, PASP, 115, 763

Chieffi, A., Limongi, M. 2002, ApJ, 577, 281

Fruchter, A.S., et al. 1999, ApJ, 519, L13

Fryer, C.L. & Woosley, S.E. 2002, ApJ, 502, L9

Fryer, C.L., Woosley, S.E., & Hartmann, D.H. 1999, ApJ, 526, 152

Fryer, C.L., Woosley, S.E., & Heger, A. 2001, ApJ, 550, 372

Fryer, C.L. 2006a, accepted by New Astronomy

Fryer, C.L. 2006b, submitted to Il Nuovo Cimento

Galama, T. J., et al. 1998,Nature, 395, 670

Heger, A., Woosley, S.E., Waters, R. 2000, in 'The First Stars." eds. Weiss, K., Abel, T, Hill, V. Springer, p. 121

Heger, A., & Woosley, S.E. 2002, ApJ, 567, 532

Heger, A., Woosley, S.E. 2003, AIPC, 662, 214

Heger, A., & Woosley, S.E. 2007, ApJ, in preparation

Heger, A., Fryer, C.L., Woosley, S.,E., Langer, N., Hartmann, D.H. 2003, ApJ, 591, 288

Hobbs, G., Lorimer, D.R., Lyne, A.G., & Kramer, M. 2005, MNRAS, 360, 974

Hurley, J. R., Pols, O. R., & Tout, C. A. 2000, MNRAS, 315, 543

Kogut, A. 2003, New Astronomy, 47, 945

Kudritzki, R.P. 2002, ApJ, 577, 389

Kulczycki, K., Bulik, T., Belczynski, K., Rudak, B., 2006, A&A in press, astro-ph/0602533

Lai, D., Rasio, F.A., & Shapiro, S.L. 1993, ApJS, 88, 205

Lamb, D.Q., & Reichart, D.E. 2000, ApJ, 536, 1

Larson, R.B. 1998, MNRAS, 301, 569

Lloyd-Ronning, N.M., Fryer, C.L., & Ramirez-Ruiz, E. 2002, ApJ, 574, 554

MacFadyen, A.I., & Woosley, S.E. 1999, ApJ, 524, 262

MacFadyen, A.I., Woosley, S.E., & Heger, A. 2001, ApJ, 550, 410

Marigo, P., Girardi, L., Chiosi, C., & Wood, P.R. 2001, A&A, 371, 152

Nakamura, F., & Umemura, M. 2001, ApJ, 548, 19

Omukai, K., & Palla, F. 2003, ApJ, 589, 677

O'Shea, B.W., Abel, T., Whalen, D., Norman, M.L. 2005, ApJ, 628, L5

O'Shea, B.W., Norman, M.L. 2006, ApJ, accepted (astro-ph/0607013)

Podsiadlowski, P., Joss, P.C., & Hsu, J.J.L. 1992, ApJ, 391, 246

Podsiadlowski, Ph., Mazzali, P.A., Nomoto, K., Lazzati, D., & Cappellaro, E. 2004, ApJ, 607, L17

Portegies Zwart, S.F., & Verbunt, F. 1996, A&A, 309, 179

Ripamonti, E., & Abel, T. 2004, MNRAS, 348, 1019

Saigo, K., Matsumoto, T., & Umemura, M. 2004, ApJ, 615, L65

Scannapieco, E., Madau, P., Woosley, S.E., Heger, A., Ferrara, A. 2005, ApJ, 633, 1031

Schaerer, D. 2002, A&A, 382, 28

Sethi, S., & Bhargavi, S.G. 2001, A&A, 376, 10

Spruit, H.C. 2002, A&A, 381, 923

Stanek, K., et al., Acta Astronomica, in press, astro-ph/0604113

Tan, J.C., & McKee, C.F. 2004, ApJ, 603, 383

Umeda, H., Nomoto, K. 2002, ApJ, 565, 385

Vreeswijk, P.M., et al. 2001, ApJ, 405, 273

Weaver, T.A., Zimmerman, G.B., Woosley, S.E. 1978, ApJ, 225, 1021

Webbink, R. F. 1984, ApJ, 277, 355

Woosley, S.E. 1993, ApJ, 405, 273

Woosley, S.E., Heger, A. 2006, ApJ, 637, 914

Woosley, S.E., Heger, A., Weaver, T.A. 2002, Rev. Mod. Phys, 74, 1015

Wyithe, S. & Loeb, A., 2003a, ApJ, 586, 693

Wyithe, S. & Loeb, A., 2003b, ApJ, 588, L69

Wyithe, S. & Loeb, A., 2004, ApJ, 612, 957

Yoon, S.-C., Langer, N. 2005, A&A, 443, 643

This preprint was prepared with the AAS LaTeX macros v5.2.

Table 1. GRB Formation Channels and Efficiencies[a]

Channel	Evolutionary Sequence[b]	η_1	η_2	η_3	η_4
grb01	MT1 GRB1 CE2 GRB2	0.0733	0.0002	0.0058	0.0063
grb02	CE1 GRB1 MT2 GRB2	0.0121	0	0	0
grb03	MT1 GRB1	0.0110	0	0	0
grb04	All others	0.0077	0	0	0
Total	All channels	0.1041	0.0002	0.0058	0.0063

[a]Formation efficiencies in case of no angular momentum constraints (η_1); MacFadyen & Woosley 1999 (η_2); this work (η_3); Podsiadlowski et al. 2004 (η_4).

[b]Notation explained in § 3.1.

Table 2. GRB Formation Efficiencies: Parameter Study[a]

Model	η_1	η_2	η_3	η_4	Description[b]
Mod01	0.1041	0.0002	0.0058	0.0063	standard
Mod02	0.1103	0	0	0	no tides
Mod03	0.0837	0.0001	0.0034	0.0037	kicks
Mod04	0.2602	0.0008	0.0147	0.0146	$M_{\rm zams,1} \geq 30$ M$_\odot$
Mod05	0.1041	0.0002	0.0058	0.0064	tides on envelope only
Mod06	0.1042	0.0002	0.0058	0.0064	$X_{\rm cou1} = 0.01$
Mod07	0.1039	0.0002	0.0058	0.0063	$X_{\rm cou1} = 1$
Mod08	0.1041	0.0242	0.0111	0.0067	$X_{\rm cou2} = 1$
Mod09	0.1041	0.0053	0.0006	0	$X_{\rm cou2} = 0.01$
Mod10	0.0831	0.0002	0.0037	0.0037	$\alpha_{\rm ce} \times \lambda = 0.3$
Mod11	0.1295	0.0001	0.0082	0.0104	$\alpha_{\rm ce} \times \lambda = 3$
Mod12	0.0471	0.0001	0.0020	0.0022	alternative IMF
Mod13	0.1030	0.0002	0.0056	0.0062	Pop I rotation
Mod14	0.1051	0.0002	0.0062	0.0068	RLOF spinup
Range	.04–.26	0–.02	0–.01	0–.01	all models

[a]Formation efficiencies in case of no angular momentum constraints (η_1); MacFadyen & Woosley 1999 (η_2); this work (η_3); Podsiadlowski et al. 2004 (η_4).

[b]Models explained in § 3.4.

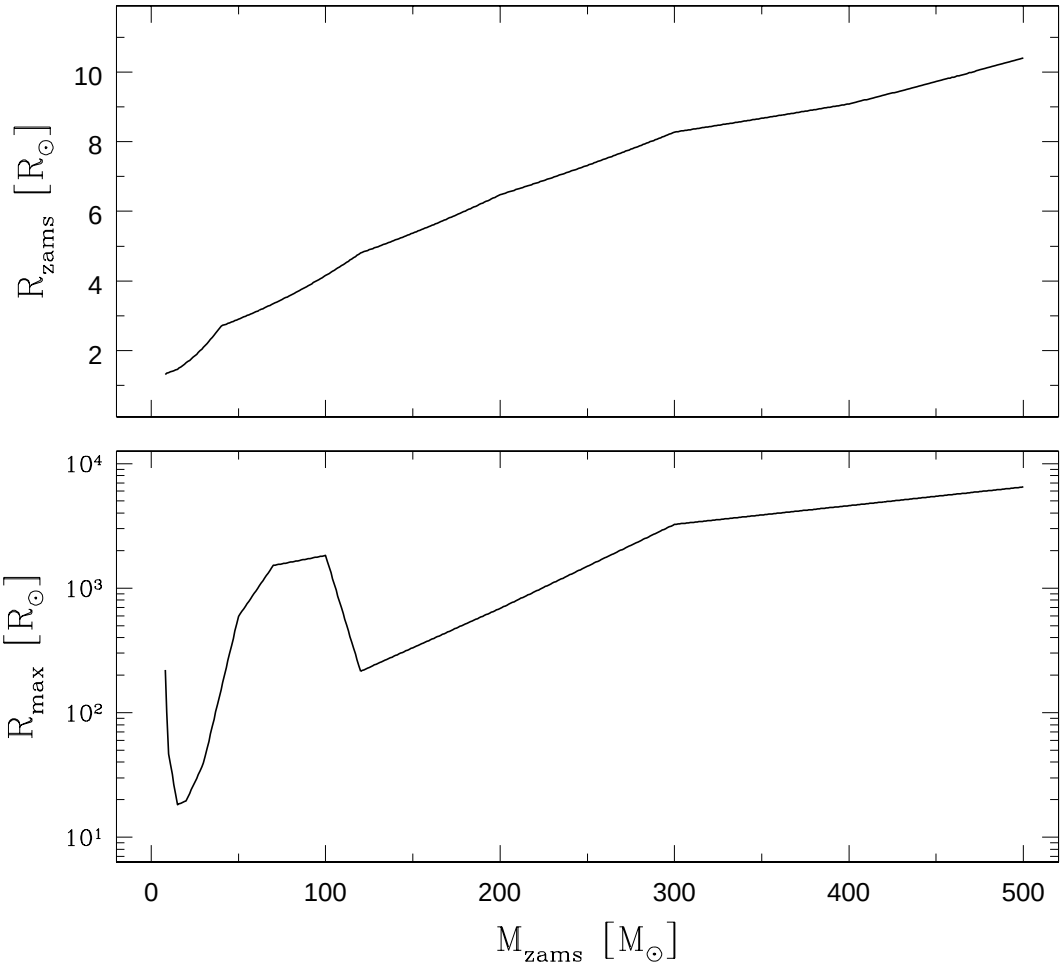

Fig. 1.— Stellar radii for Population III stars; top panel shows initial (ZAMS) radii, while bottom panel shows maximum radii. For details see § 2.

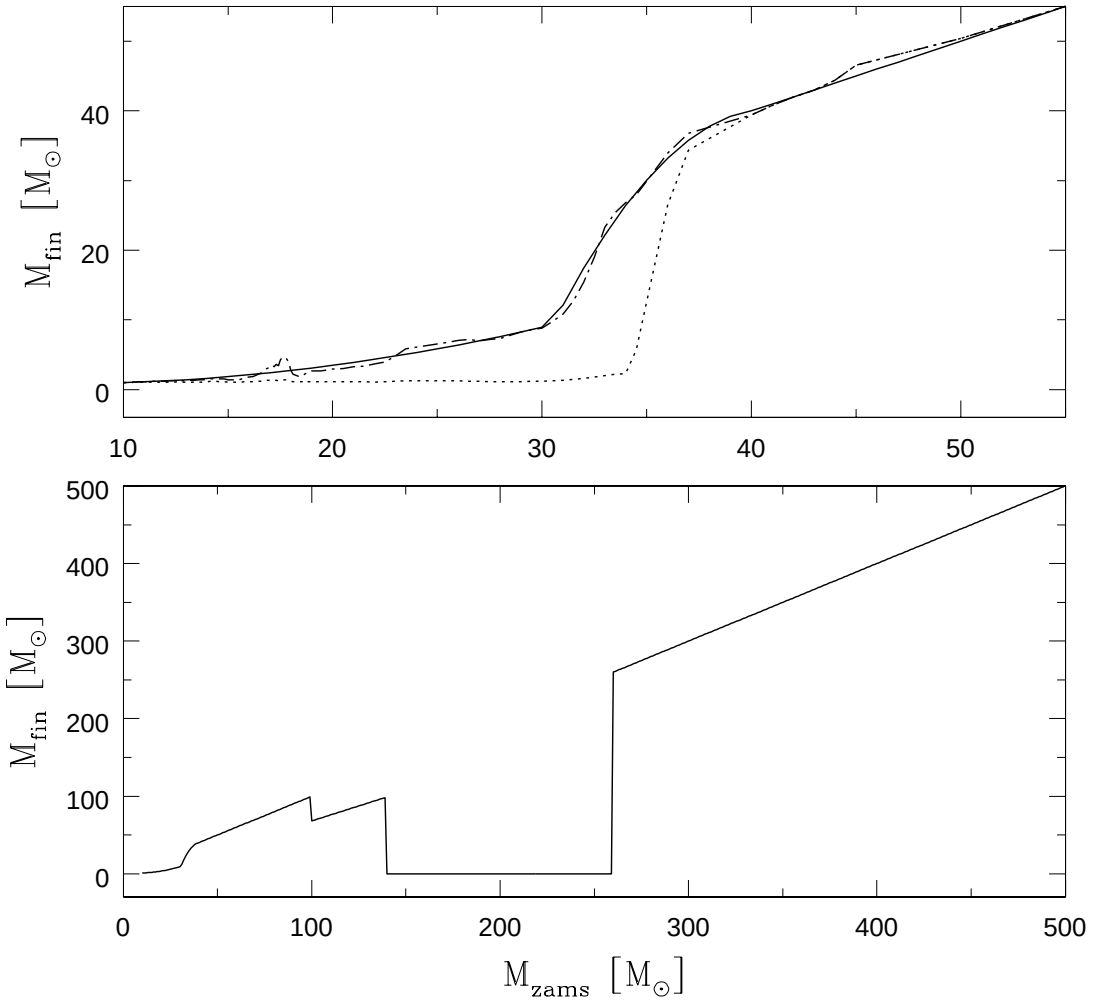

Fig. 2.— Initial-final mass relation for Population III stars. Bottom panel: our best fit to the Fryer (2006) models (see eq. 7). Top panel: comparison with the Fryer (2006) models. Initial (before fallback) and final remnant masses are shown with dotted and dashed lines, respectively. Solid line indicates the fit used in this study. Note that for stars below $\sim 35\,M_\odot$, the bulk of the remnant mass arises from fallback. Note also that because the structure of the star changes radically between 15 and $20\,M_\odot$, so does the remnant mass.

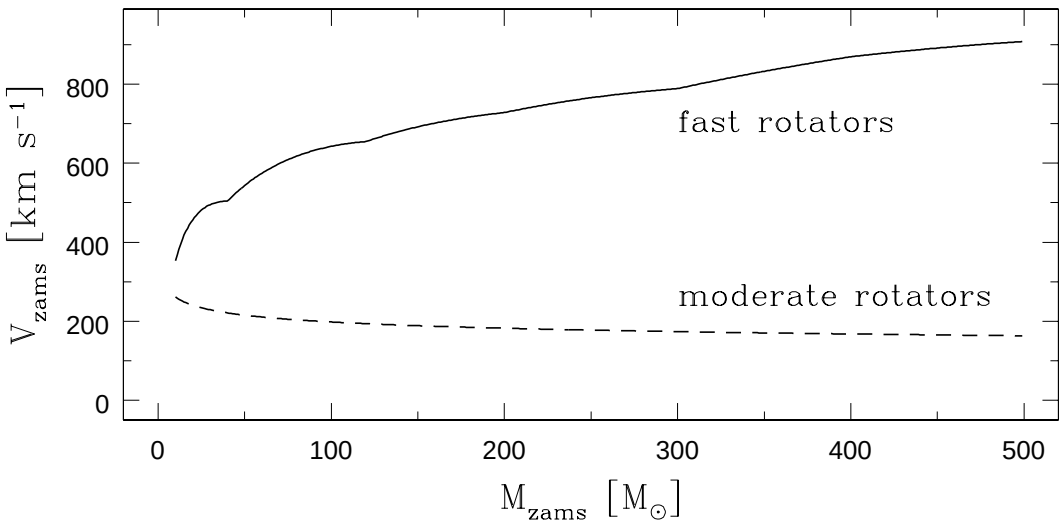

Fig. 3.— Initial rotational velocities adopted for Population III stars. We use either 30% of the Keplerian velocity (fast rotators), or we use the estimates derived for Population I stars (moderate rotators).

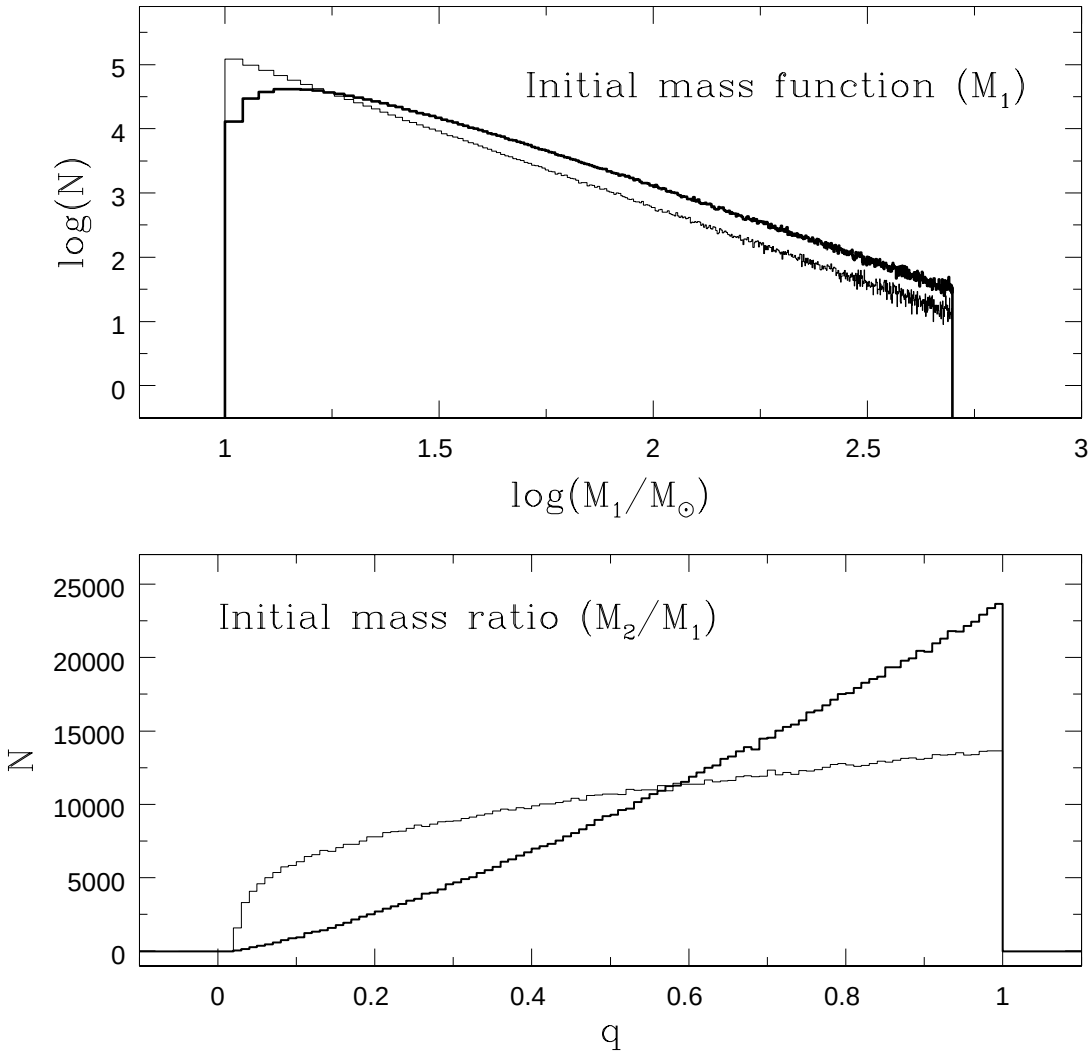

Fig. 4.— Initial mass function and initial mass ratio distribution for Population III stars; standard model (thick lines) and alternative IMF model (thin lines) are presented. For details see § 2.6.

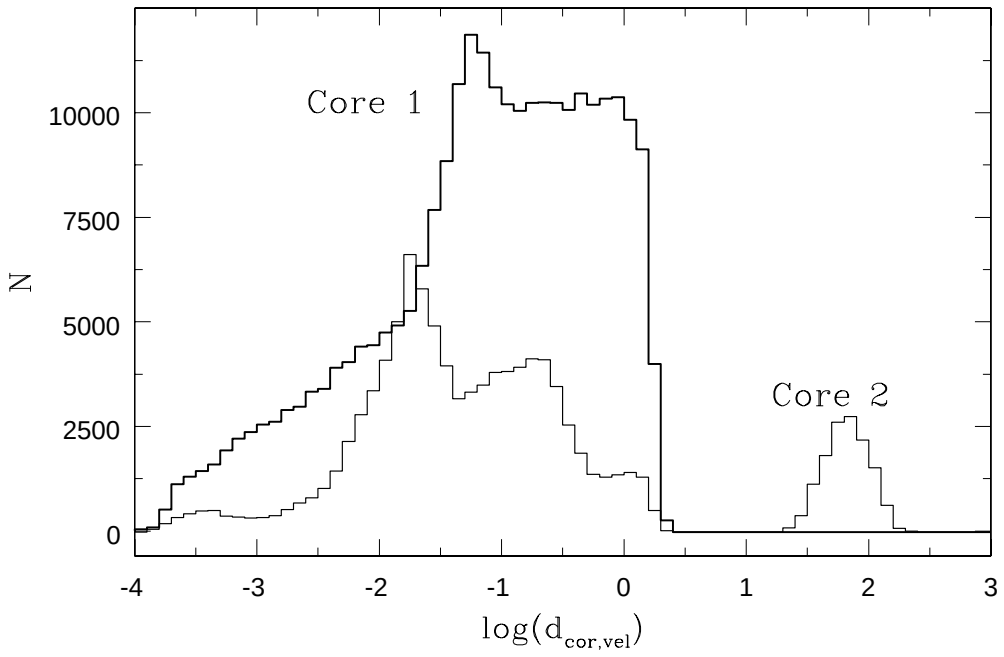

Fig. 5.— Effects of tides (synchronization) on core angular velocity. A core of a binary component is generally slowed down (speed changes by factor of $d_{\rm cor,vel} \sim 0.01 - 1$) if tidal forces are allowed to work on entire star. Core speed change for a primary (core 1) and a secondary star (core 2) are presented. Note a subpopulation of secondary cores that are spun up by factors of $d_{\rm cor,vel} \sim 30 - 100$. For details see § 2.4.

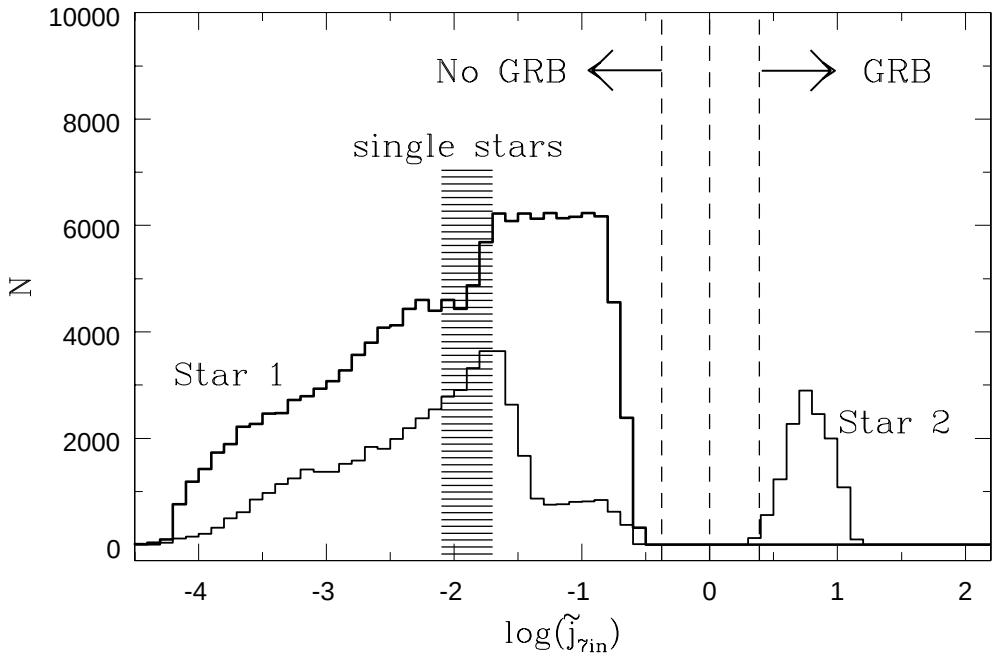

Fig. 6.— Specific angular momentum of potential GRB progenitors from Population III binaries: primary is marked as Star 1, while secondary as Star 2. Potential progenitors are these stars that are stripped of their envelopes and are massive enough to form BH (but no constrain is put on their specific angular momentum). For comparison we plot the range (shaded area) of specific angular momentum for Population III single stars (these which in the end form black holes). We also mark (dashed lines) the minimum specific angular momentum required to produce GRB for three different criteria used in this work (see eq. 26). Note that only a subpopulation of secondary stars with rather high specific angular momentum ($\tilde{j} \gtrsim 1$) will produce GRB.

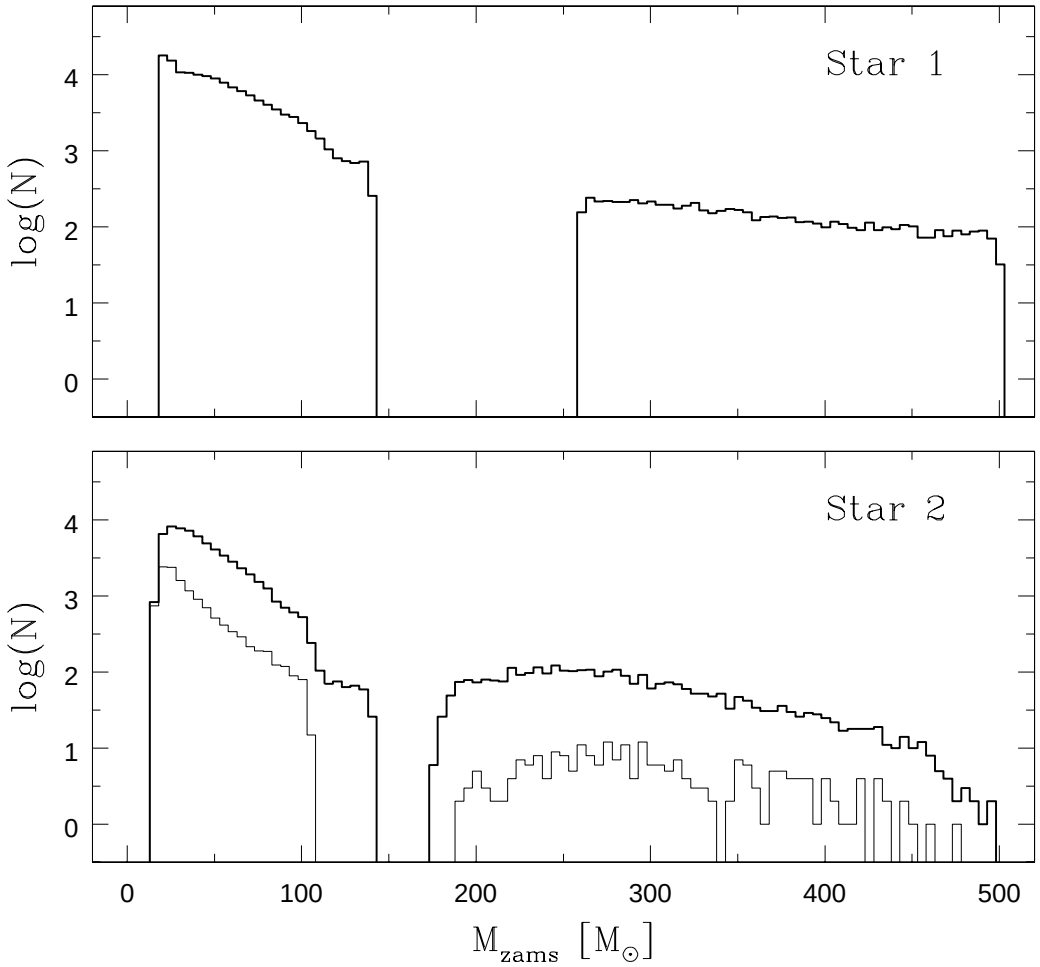

Fig. 7.— Distribution of initial (ZAMS) masses in potential (naked helium stars massive enough to form BH) GRB binary progenitors. Potential progenitors are these stars that are stripped of their envelopes and are massive enough to form BH (but no constrain is put on their specific angular momentum). Primary components are shown in the top panel, while secondaries in the bottom panel. Progenitors that produce cores with specific angular momentum ($\tilde{j} \gtrsim 1$) high enough to make GRB are shown with the thin line.

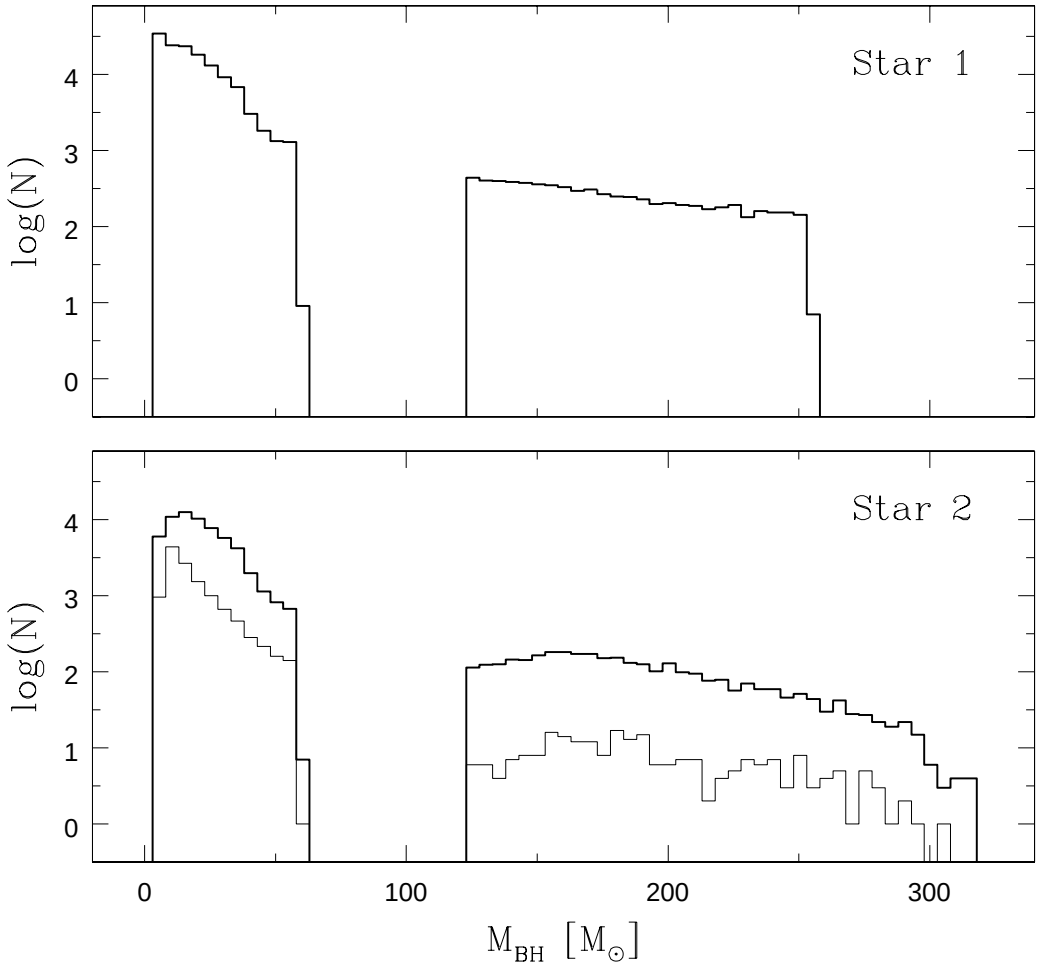

Fig. 8.— Distribution of final remnant (BH) masses in potential GRB binary progenitors. Potential progenitors are these stars that are stripped of their envelopes and are massive enough to form BH (but no constrain is put on their specific angular momentum). Remnants from a primary component are shown in the top panel, while from secondaries in the bottom panel. Progenitors with specific angular momentum ($\tilde{j} \gtrsim 1$) high enough to produce GRB are shown with the thin line. Note that only small fraction of secondaries can produce a GRB.

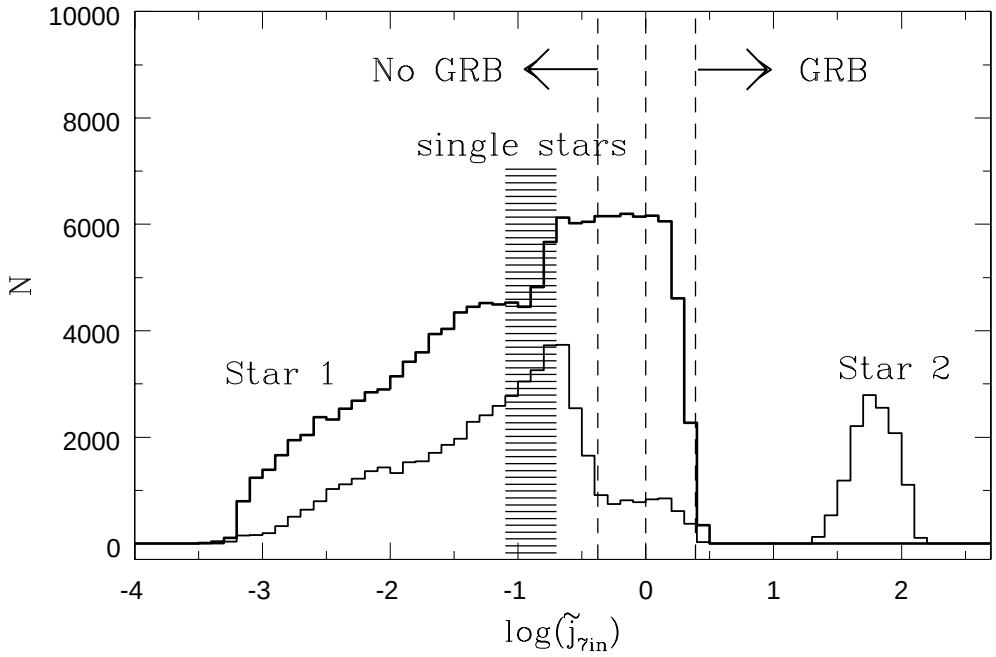

Fig. 9.— Specific angular momentum of potential GRB progenitors for model with no angular momentum loss from the inner core (no coupling for iron core; $X_{\rm cou2} = 1$). Note that, in contrast to the standard model, both primary and secondary can make a GRB. Notation as in Figure 6.